JCB Journal of Cell Biology

ARTICLE

B cell mechanotransduction via ATAT1 coordinates actin and lysosomal dynamics at the immune synapse

Pablo Aceitón[1*], Isidora Riobó[1*], Felipe Del Valle Batalla[1*], Jheimmy Diaz-Muñoz[1], Romina Ulloa[1], Fernanda Cabrera Reyes[1], Teemly Contreras[1], Sara Hernández-Pérez[2,3,4], Pieta K. Mattila[2,3,4], and María Isabel Yuseff[1]

B cells extract immobilized antigens via immune synapse formation, a process influenced by the physical properties of the antigen-presenting surface. However, the mechanisms linking mechanotransduction to antigen extraction and processing remain poorly understood. Here, we show that B cells activated on stiff substrates initiate mechanotransduction responses that drive the translocation of the microtubule acetylase ATAT1 from the nucleus to the cytoplasm, leading to increased α-tubulin acetylation. This modification releases GEF-H1 at the immune synapse, where it promotes the formation of actin foci essential for antigen extraction. Acetylated microtubules also enable B cells to stabilize and position lysosomes at the synapse center, thereby coupling actin-dependent extraction to antigen processing and presentation. Accordingly, ATAT1-silenced B cells fail to concentrate actin foci and lysosomes at the synaptic interface, resulting in impaired antigen extraction and presentation to T cells. Overall, these findings underscore how BCR-dependent mechanotransduction induces microtubule modifications to orchestrate lysosome positioning and actin remodeling at the immune synapse.

Introduction

Mechanosensing is a fundamental cellular process that enables cells to perceive and respond to physical environmental cues (Shaheen et al., 2019). This ability allows cells to adapt to tissue geometry and stiffness (also referred to as rigidity, measured in kPa), which in turn can influence genetic reprogramming, cell adhesion, migration, and organelle function (Chen et al., 2017; Lachowski et al., 2022; Phuyal et al., 2022). How mechanical cues associated with antigen recognition by B cells dictate their activation remains unresolved.

B cells interact with antigens that display diverse mechanical properties, ranging from less stiff immune complexes to highly rigid viral capsids (~100 MPa) (Shaheen et al., 2019). Additionally, B cells can recognize antigens in a soluble form, considered to be in an environment with extremely low stiffness (0.01 kPa), or interact with antigens associated to the extracellular matrix, which displays rigidities within 20 kPa (Ciechomska et al., 2014). In vivo, B cells mainly interact with antigens tethered to the plasma membrane of antigen-presenting cells, exhibiting diverse rigidities (0.1–0.5 kPa) that are modified by inflammatory conditions (Bufi et al., 2015; Kim et al., 2019).

B cells display a membrane-bound immunoglobulin receptor, the B cell receptor (BCR), which possesses the ability to sense the mechanical properties of their ligands (Zhu et al., 2019b; Zhu et al., 2019a). Accordingly, B cells activated on stiff surfaces exhibit augmented BCR clustering and downstream signaling, leading to enhanced spreading responses and actin cytoskeletal rearrangements (Wan et al., 2013). Consequently, external physical cues provide an additional layer of information that B cells can detect and integrate into their responses. However, how B cells couple mechanotransduction pathways with membrane trafficking to regulate antigen extraction and presentation under varying conditions at the immune synapse (IS) remains incompletely understood.

The mode of antigen extraction used by B cells depends on the physical properties of the substrate in which antigens are presented: antigens on flexible, softer surfaces are internalized into clathrin-coated pits by myosin IIA-mediated pulling forces that trigger invagination of antigen-containing membranes (Hoogeboom and Tolar, 2016). During this process, the complexes formed by the BCR and the antigen are internalized at regions enriched in actin foci (Roper et al., 2019). On the other

[1]Laboratory of Immune Cell Biology, Department of Cellular and Molecular Biology, Pontificia Universidad Católica de Chile, Santiago, Chile; [2]Institute of Biomedicine, and MediCity Research Laboratories, University of Turku, Turku, Finland; [3]Turku Bioscience, University of Turku and Åbo Akademi University, Turku, Finland; [4]InFLAMES Research Flagship Center, University of Turku, Turku, Finland.

*P. Aceitón, I. Riobó, and F. Del Valle Batalla contributed equally to this paper. Correspondence to María Isabel Yuseff: myuseff@uc.cl.

https://doi.org/10.1083/jcb.202407181

hand, antigens presented on more rigid surfaces require the local fusion of lysosomes at the synaptic membrane that release proteases and acidify the synaptic cleft, facilitating antigen extraction (Yuseff et al., 2011). This proteolytic mode of antigen extraction relies on the precise positioning, tethering, and secretion of lysosomal content at the IS. Various factors regulate this process, including local actin cytoskeleton remodeling by proteasome activity (Ibañez-Vega et al., 2019a), assembly of the exocyst complex (Sáez et al., 2019), and VAMP7-dependent fusion at the synaptic membrane (Obino et al., 2017). However, the mechanisms that link mechanotransduction to lysosome positioning remain largely unknown, and B cells emerge as a valuable model to study this process.

Vesicles move along microtubules (MTs) by their association to motor proteins, which can be regulated by posttranslational modifications (PTMs) of the MT network (Pu et al., 2016). In neurons, acetylation of MTs fine-tunes the trafficking of lysosomes by modifying their affinity with kinesins (Morelli et al., 2018). In T cells, upregulation of tubulin acetylation by inhibition of the deacetylase HDAC6 leads to impaired transport of lytic granules to the synaptic membrane, highlighting how MT acetylation impacts polarized vesicle transport (Núñez-Andrade et al., 2016). Moreover, PTMs of the MT network are also coupled to mechanoresponses, resulting in differential trafficking of vesicles to sites where membrane exchange or exocytosis is required (Wang et al., 2018). For instance, acetylation of tubulin is enhanced at the leading edge of migrating fibroblasts where traction forces occur, promoting the release of GEF-H1 and actomyosin contractibility to modulate focal adhesion dynamics at the cell front (Seetharaman et al., 2022). Similarly, the localized release and activation of GEF-H1 by MTs at the synaptic membrane of B cells restricts F-actin polymerization, thereby ensuring the formation and stability of a single IS (Pineau et al., 2022). This underscores the coordinated interplay between actin and MTs in maintaining cellular polarity across diverse cellular contexts.

In this work, we show that the activation of B cells on stiffer substrates enhances the concentration of lysosomes at the center of the IS, ultimately improving their capacity to extract and present immobilized antigens. This process relies on a B cell response that triggers the translocation of the acetylase α-tubulin (α-Tub) acetyltransferase 1 (ATAT1) from the nucleus to the cytoplasm, thereby increasing tubulin acetylation levels. Concomitantly, increased levels of acetylated MTs also trigger the release of GEF-H1, which accumulates at the synaptic membrane to stabilize the formation of actin foci, where antigen extraction occurs. Altogether, our findings reveal how physical properties of antigen-presenting surfaces can regulate the formation of a functional IS and thereby tune B cell effector responses.

Results

The stiffness of antigen-presenting surfaces regulates actin remodeling and mechanotransduction pathways in B cells

Upon interaction with surface-tethered antigens, B cells trigger a spreading response to maximize antigen encounter and uptake (Fleire et al., 2006; Yuseff et al., 2013). In this study, we aimed to characterize cytoskeletal and vesicular responses coupled to mechanical cues sensed through the BCR. For this purpose, we developed polyacrylamide (PAA) gels of 0.3 and 13 kPa, hereafter referred to as "soft" and "stiff" gels, respectively, which mimicked physical cues associated to physiological and pathological conditions (Wan et al., 2013) (Fig. S1 A). The stiffness of these gels was measured by atomic force microscopy (AFM) (Fig. S1 B) to confirm soft and stiff values. Next, BCR$^+$ ligands (F(ab′)2 anti-IgG) were coupled to both soft and stiff gels, which exhibited similar binding densities and formed a continuous and homogeneous layer under all conditions (Fig. S1 C). B cells were seeded on gels containing BCR$^+$ ligands for various time points, then fixed and stained for actin and YES-associated protein (YAP), a well-established mechanotransduction marker that translocated to the nucleus in response to mechanical cues (Cheng et al., 2023). Our results confirmed that B cells exhibit key mechanotransduction responses, as YAP translocated to the nucleus in cells activated on stiffer substrates, but not on softer ones (Fig. 1, A and B). This translocation occurred in a time-dependent manner, consistent with observations in other cell types (Panciera et al., 2017). We also evaluated the active form of pFAK, a well-established hallmark of mechanotransduction in B cells (Shaheen et al., 2017) and in other cell types where it is associated with focal adhesion assembly and membrane protrusion during cell spreading and migration (Li et al., 2023). For this purpose, we activated B cells on surfaces with different stiffnesses for increasing time points and evaluated the levels of pFAK by immunoblot. Our results show that cell lysates from B cells activated on stiff surfaces display increased levels of pFAK (Fig. 1 C). Accordingly, B cells seeded over stiff substrates containing BCR$^+$ ligands exhibited higher spreading responses after 15 and 30 min in comparison with those activated on softer substrates (Fig. 1 D). Mean areas of B cells activated under stiff conditions were in the range of 300–400 μm^2 compared with an average of 100 μm^2 for B cells activated under soft conditions (Fig. 1 E). Notably, B cells seeded onto gels of different stiffness without BCR$^+$ ligands showed no significant changes in spreading after 5 and 30 min (Fig. S1, D and E). These observations suggest that B cells possess a BCR-dependent mechanotransduction pathway that controls cell spreading in response to substrate rigidity when coupled to BCR$^+$ ligands.

When examining actin cytoskeleton organization, we observed an increase in lamellipodia size and the number of actin foci (Fig. 1 F & right inset, Fig. 1, F and G) in B cells activated on stiffer substrates, compared with those on soft substrates, which did not display well-defined lamellipodia. Actin foci are dynamic actin-rich structures that are considered a hallmark of B cell mechanoresponses as they generate inward forces that facilitate antigen concentration and internalization (Roper et al., 2019). We also verified that B cells induce stronger BCR signaling responses when activated on stiffer versus soft substrates (Fig. S2 A). Immunoblot analysis revealed that B cells displayed higher levels of phospho-AKT and phospho-ERK when activated on stiffer substrates in comparison to softer conditions, as previously described (Shaheen et al., 2019). These observations show that BCR-mediated mechanotransduction in response to

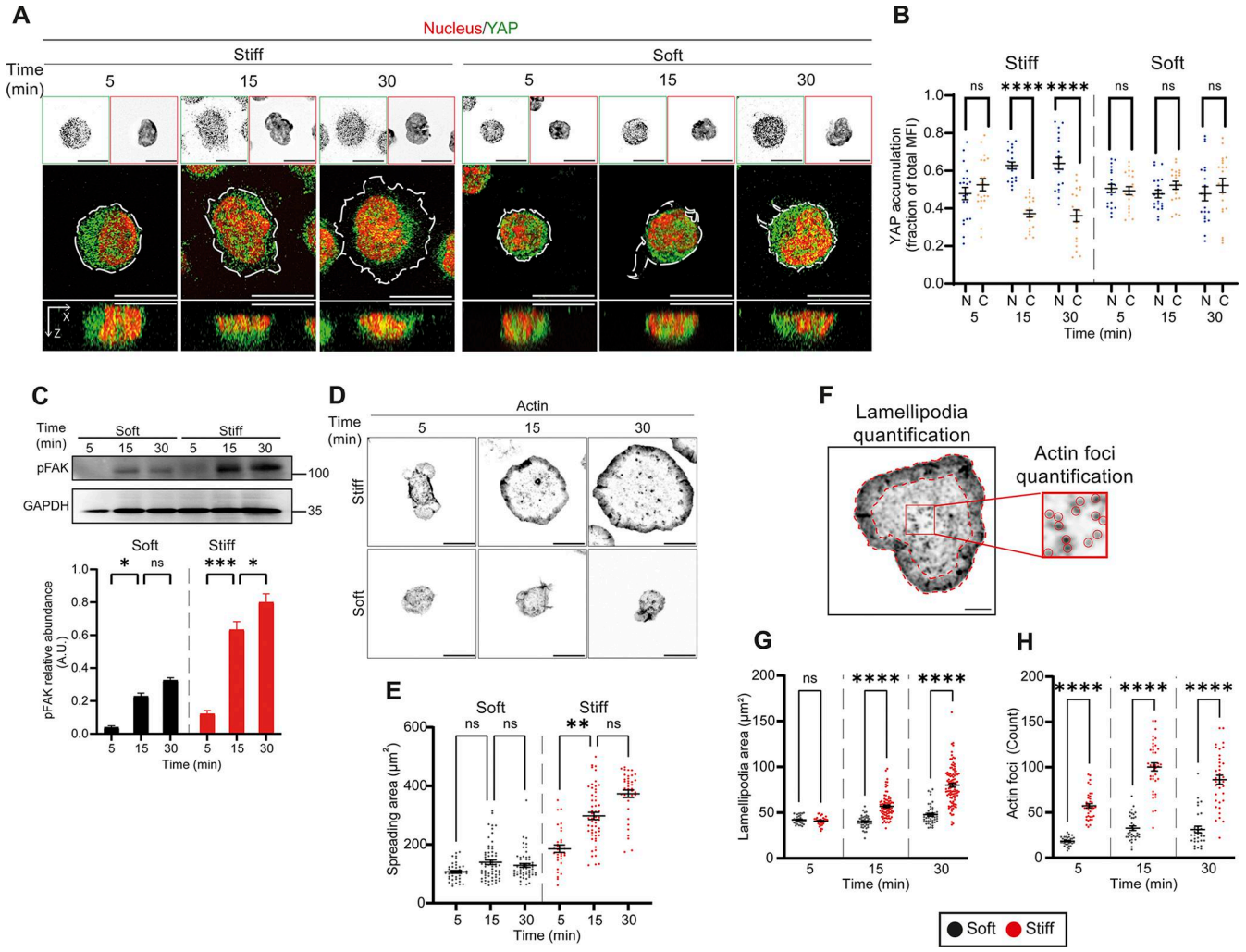

Figure 1. **The stiffness of the antigen-presenting surfaces regulates actin remodeling and mechanotransduction pathways in B cells. (A)** Representative images of fixed B cells seeded over stiff or soft substrates containing BCR⁺ ligands at different activation times. YAP is shown in green, the nucleus in red (Hoechst). **(B)** Quantification of nuclear or cytoplasmic accumulation of YAP from cells in A. The distribution index (y axis) indicates the fraction of YAP fluorescence in the nucleus (N) or the cytoplasm (C), excluding the nucleus, with respect to the total area of the cell. **(C)** Western blot analysis of phosphorylated FAK (pFAK) in B cells activated on soft or stiff substrates for different time points. Bottom: Quantification of pFAK shows significantly higher levels in B cells activated on stiff substrates. **(D)** Representative images of B cells seeded over stiff or soft substrates containing BCR⁺ ligands at different activation times. Actin (phalloidin) is shown on a gray scale. **(E)** Quantification of cell spreading areas. **(F)** Representative selection of lamellipodia and actin foci used for quantification. **(G and H)** Results are shown in G and H. For every experiment, shown data consider $n > 20$ cells pooled from $N = 3$ independent experiments. Scale bars are 10 μm. Two-way ANOVA with Sidak's multiple comparison test. P values illustrated with asterisks are ** <0.01, *** <0.001, and **** <0.0001. Error bars are mean ± SEM. Source data are available for this figure: SourceData F1.

substrate stiffness activates FAK and BCR downstream signaling molecules that regulate spreading and signaling pathways associated with enhanced states of B cell activation. Collectively, these findings support the notion that mechanical cues modulate actin cytoskeleton remodeling initiated by BCR engagement, prompting us to investigate how B cells integrate physical signals to regulate antigen extraction and presentation.

Mechanostransduction regulates lysosome positioning and dynamics at the IS

B cells strategically position lysosomes at the IS to promote the uptake and processing of antigens; therefore, we asked whether physical cues sensed by B cells have an impact on lysosome positioning and dynamics. For this, we seeded B cells on soft or stiff substrates containing BCR⁺ ligands at increasing time points. Cells were stained for F-actin and the lysosomal marker LAMP1 and imaged using confocal microscopy (Fig. 2 A). The distribution of LAMP1⁺ vesicles within the intracellular space defined by cortical actin cytoskeleton was analyzed as follows: the total cell area was divided into 3 concentric sections, defining the center and periphery as previously described (Corrales Vázquez et al., 2025) (Fig. 2 B) and raw intensity fluorescence values of LAMP1⁺ vesicles, referred to as lysosomes, at the central and peripheral regions were normalized with respect to the spreading area of each cell. Our analysis revealed that after 15 min of activation, B cells stimulated on stiff surfaces progressively accumulated more lysosomes at the center of the IS compared with cells activated on softer substrates. The number

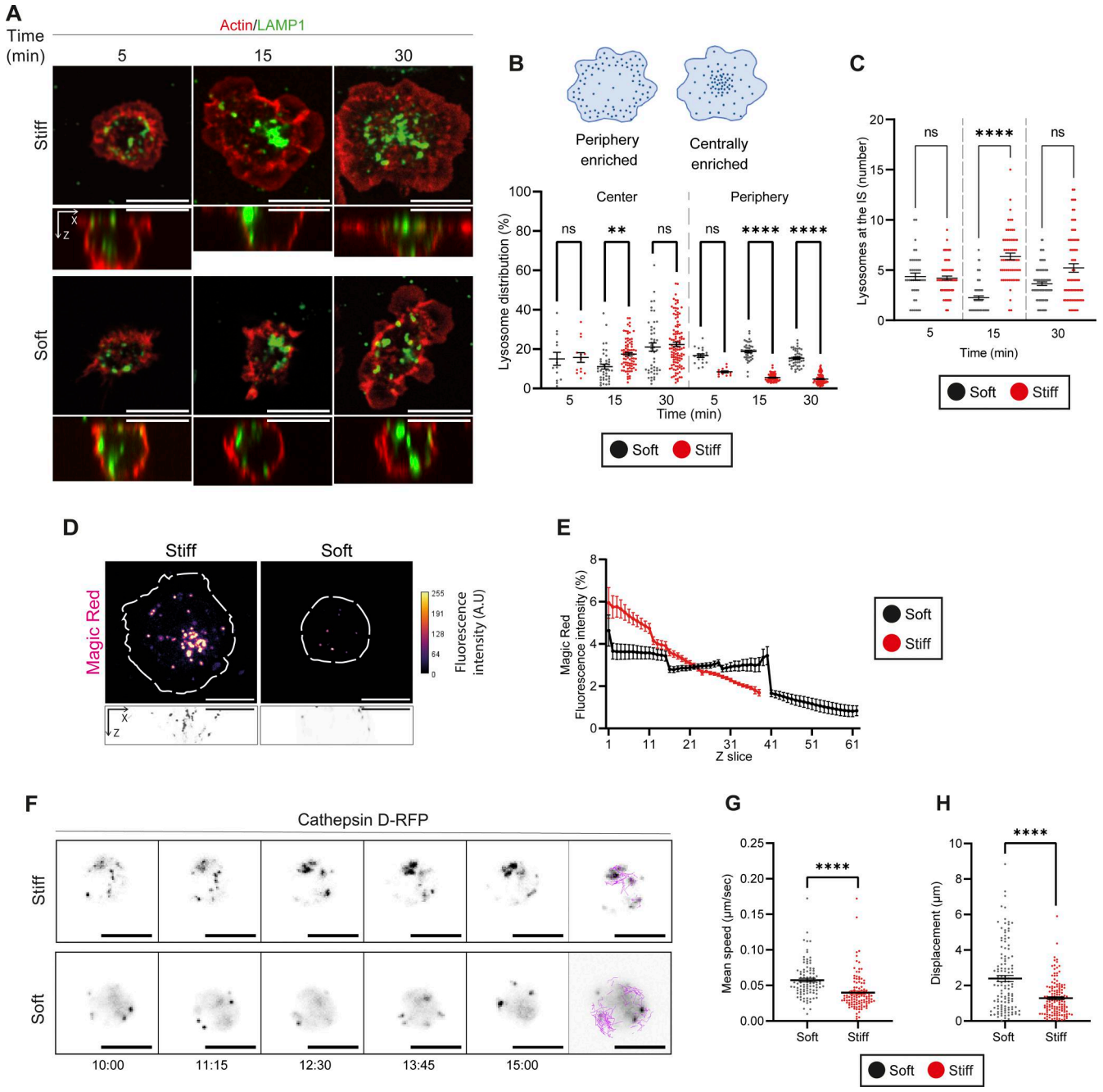

Figure 2. **Mechanotransduction associated to lysosome localization and dynamics during B cell activation. (A)** Representative images of fixed B cells interacting with soft or stiff substrates containing BCR⁺ ligands at different time points. LAMP1 is shown in green, and the cell border (white dashed outline) was defined by F-actin phalloidin staining. Scale bar: 10 µm. **(B)** Top: Schematics depicting central and peripheral areas of the IS where LAMP1⁺ lysosomes were quantified. (see Materials and methods). Bottom: Represents the MFI percentage of LAMP1⁺ lysosomes in each region. **(C)** Number of lysosomes at the IS from cells shown in A. **(D)** Representative images of MR signal in B cells seeded on soft or stiff substrates containing BCR⁺ ligands. **(E)** MR fluorescence intensity through Z stacks for cells displayed in D. **(F)** Representative time-lapse images of B cells expressing cathepsin-RFP activated on stiff or soft conditions. **(G and H)** Displacement and mean speed of lysosome tracks from cells detailed in F. Data shown consider $n \geq 30$ cells pooled from $N = 3$ independent experiments. Scale bars are 10 µm. **(B and C)**: Two-way ANOVA with Sidak's multiple comparison test. **(G and H)**: *t* test. P values illustrated with asterisks are ** <0.01, *** <0.001, and **** <0.0001. Error bars are mean ± SEM.

of lysosomes at the center of the IS was comparable in both conditions after 30 min of activation. However, the number of lysosomes at the periphery was significantly lower in B cells interacting with stiffer substrates, suggesting that the lysosomes are retained more efficiently at the center of the synapse in cells activated on surfaces with higher stiffness (Fig. 2 B). No differences were observed in total LAMP mean fluorescence in B cells activated in either condition (Fig. S3 C); however, quantification of LAMP1⁺ vesicles at the z-plane adjacent to the antigen-coated surface revealed higher number of lysosomes at the synaptic

plane of B cells activated on stiffer substrates after 15 min of activation (Fig. 2, A and C), suggesting that lysosomes were recruited more efficiently.

We next monitored the lysosome hydrolase activity in B cells activated on stiff and soft substrates. To this end, we incubated B cells on activating surfaces for 30 min and added the cathepsin B–sensitive probe, Magic Red (MR), which penetrates cells and fluoresces upon cleavage within catalytically active lysosomes (Barral et al., 2022). Imaging analysis revealed that B cells accumulate higher MR fluorescence at the synaptic plane when activated on stiff substrates (Fig. 2 D). Additionally, these cells display more MR puncta at the center of the synapse compared with cells activated on soft substrates, where puncta were more peripherally located (Fig. 2 E), similarly to our observations with LAMP1$^+$ vesicles. These results suggest that lysosomes with higher degrative activity are recruited to the center of the IS upon activation with antigens associated to stiff substrates.

We next evaluated how substrate stiffness sensed by B cells regulates lysosome dynamics upon formation of an IS. To this end, B cells expressing cathepsin D-RFP were seeded on soft or stiff substrates coupled to BCR$^+$ ligands for 15 min and live imaging was performed for 5 min (Fig. 2 F and video 1), a time frame suitable to evaluate lysosome dynamics during the IS formation (Sáez et al., 2019). Consistent with the results obtained in fixed cells, lysosomes preferentially accumulated to the cell center upon activation under stiff conditions, whereas on softer substrates, lysosomes were evenly dispersed. Quantitative analysis of lysosomal dynamics at the IS revealed that both mean speed and displacement were reduced in B cells seeded on stiffer substrates compared with softer ones (Fig. 2, G and H). These results suggest that increased responses to substrate stiffness promote lysosome stabilization at the IS, which could potentially impact the capacity of B cells to extract and present immobilized antigens. Thus, we next investigated the mechanisms linking lysosome dynamics to mechanotransduction in B cells.

B cell mechanotransduction promotes tubulin acetylation during activation

Intracellular trafficking relies on the organization of the MT network, where PTMs of tubulin tune MT dynamics and regulate vesicle transport (Janke and Magiera, 2020). Whether physical cues impact lysosome transport at the IS through MT PTMs remained to be determined. One such modification is the acetylation of α-Tub at lysine 40, which stabilizes the tubulin lattice and ensures the binding of KIF proteins that promote synaptic vesicle transport in neurons (Bhuwania et al., 2014). Thus, we evaluated whether physical cues sensed by B cells through their BCR can change the level of MT acetylation. To this end, B cells were seeded over soft or stiff BCR$^+$-coupled PAA gels for 5, 15, and 30 min and stained for α-Tub and acetylated tubulin (Ac-Tub). Noticeably, B cells activated on stiff surfaces displayed higher levels of Ac-Tub compared with cells activated on soft substrates (Fig. 3 A), which was measured as the total amount of Ac-Tub and as a ratio to total tubulin levels (Fig. 3, B and C). This result was confirmed by western blot analysis of cell lysates from B cells activated on stiff and soft substrates, showing that levels of Ac-Tub were upregulated in a time- and stiffness-dependent manner (Fig. S2 B).

To investigate the functional impact of MT acetylation on lysosome dynamics, we first evaluated the colocalization of Ac-Tub and LAMP1 in B cells activated on soft and stiff substrates. Our results show that in B cells seeded on stiff substrates, lysosomes progressively increased their association with Ac-Tub (Fig. 3, D and E), whereas this parameter remained constant in B cells activated on soft substrates. These results suggest that there is a functional link between MT acetylation during B cell mechanoresponses and the positioning of lysosomes at the IS during B cell activation.

To precisely determine the effect of tubulin acetylation on lysosome dynamics in B cells, we evaluated the effect of suberanilohydroxamic acid (SAHA), which enhances tubulin acetylation by inhibiting the deacetylase enzyme HDAC6 (Sáez et al., 2019). Treatment with 1 μM SAHA for 30 min effectively led to enhanced MT acetylation in B cells (Fig. S2 C). Next, B cells expressing cathepsin D-RFP treated or not with SAHA, were activated on stiff and soft surfaces for 15 min and imaged during 5 min at 8 s per frame. Lysosome trajectories from each cell under different conditions were acquired and analyzed. Our results show that lysosomes from SAHA-treated B cells activated on soft substrates exhibited lower mean speed and were more confined compared with lysosomes from non-treated cells, displaying readouts similar to lysosomes from B cells activated on stiff substrates (Fig. 3, F and H; and video 2). Interestingly, treatment with SAHA had no significant effect on lysosome dynamics in B cells activated on stiff substrates, indicating that the level or threshold of tubulin acetylation to control lysosome mobility and positioning in B cells activated on stiff substrates cannot be further increased by inhibiting deacetylation of MTs. Overall, this result suggests that tubulin acetylation can adjust lysosome dynamics in B cells as a response to extracellular stiffness.

ATAT1-mediated tubulin acetylation controls lysosome positioning in B cells

Having shown that tubulin acetylation levels modulate lysosome dynamics, we sought to elucidate the regulatory mechanisms involved. Tubulin acetylation is mediated by the acetyltransferase ATAT1, which dynamically shuttles between the nucleus and cytoplasm (Deb Roy et al., 2022). Since tubulin acetylation increases in response to substrate stiffness during B cell activation, we investigated whether this process is driven by the cytoplasmic accumulation of ATAT1. To this end, we seeded B cells on soft and stiff substrates and evaluated the localization of ATAT1 by confocal microscopy after different time points of activation. With increasing activation times and substrate stiffness, ATAT1 translocated from the nucleus to the cytoplasm, which was not observed in B cells activated on soft substrates (Fig. 4, A and B). These results suggest that BCR-mediated mechanotransduction may enhance tubulin acetylation by promoting the cytoplasmic localization of ATAT1.

To formally show that ATAT1-dependent MT acetylation regulates lysosome dynamics in B cells, we silenced ATAT1 expression using siRNA and evaluated its effect over tubulin

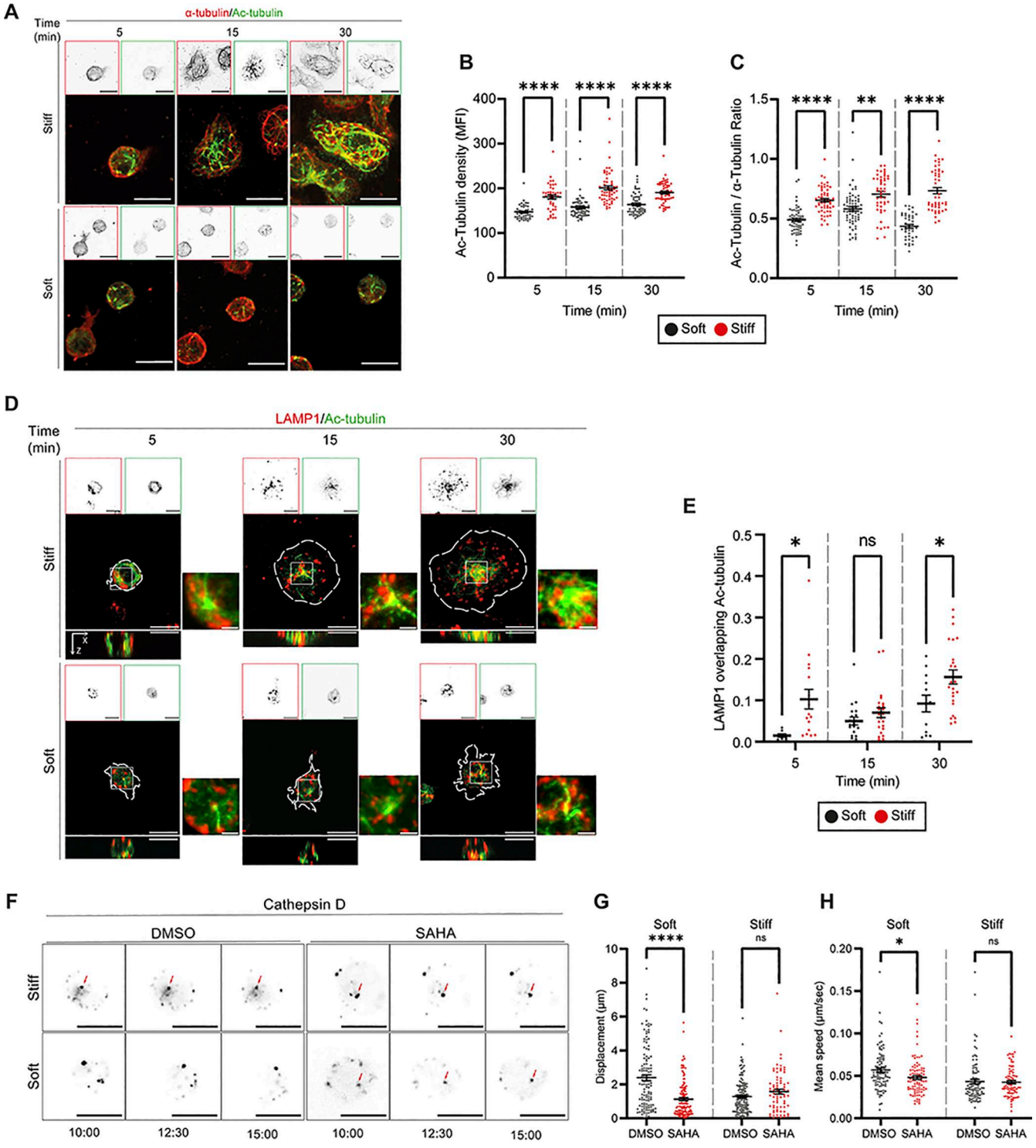

Figure 3. **B cells activated on stiff substrates display enhanced tubulin acetylation and central clustering of lysosomes at the IS. (A)** Representative images of fixed cells activated on soft or stiff substrates at different time points stained for α-Tub (red) and Ac-Tub (green). **(B)** Ac-Tub density calculations based on MFI at the IS for images in A. **(C)** Ac-Tub/α-Tub MFI ratios quantified at the IS for images in A. **(D)** Representative images of B cells seeded over stiff or soft substrates at different activation times. Ac-Tub is shown in green, LAMP1 in red, and the cell border (white dashed outline) was defined by F-actin phalloidin staining. **(E)** Quantification of lysosome accumulation on acetylated MT tracks from cells shown in D using Manders overlap coefficient. **(F)** Representative time-lapse images showing the tracking of cathepsin D$^+$ lysosomes from cells activated on either stiff or soft conditions control (non-treated—NT) cells and SAHA-treated cells. Lysosome tracks were followed for 5 min after seeding the cells for 15 min. **(G and H)** Displacement and mean speed of lysosome tracks for experiments detailed in F. Data shown consider $n \geq 30$ cells pooled from $N = 3$ independent experiments. Scale bars are 10 μm. Inset scale bars are 2 μm. Two-way ANOVA with Sidak's multiple comparison test. P values illustrated with asterisks are * <0.05, ** <0.01, and **** <0.0001. Error bars are mean ± SEM.

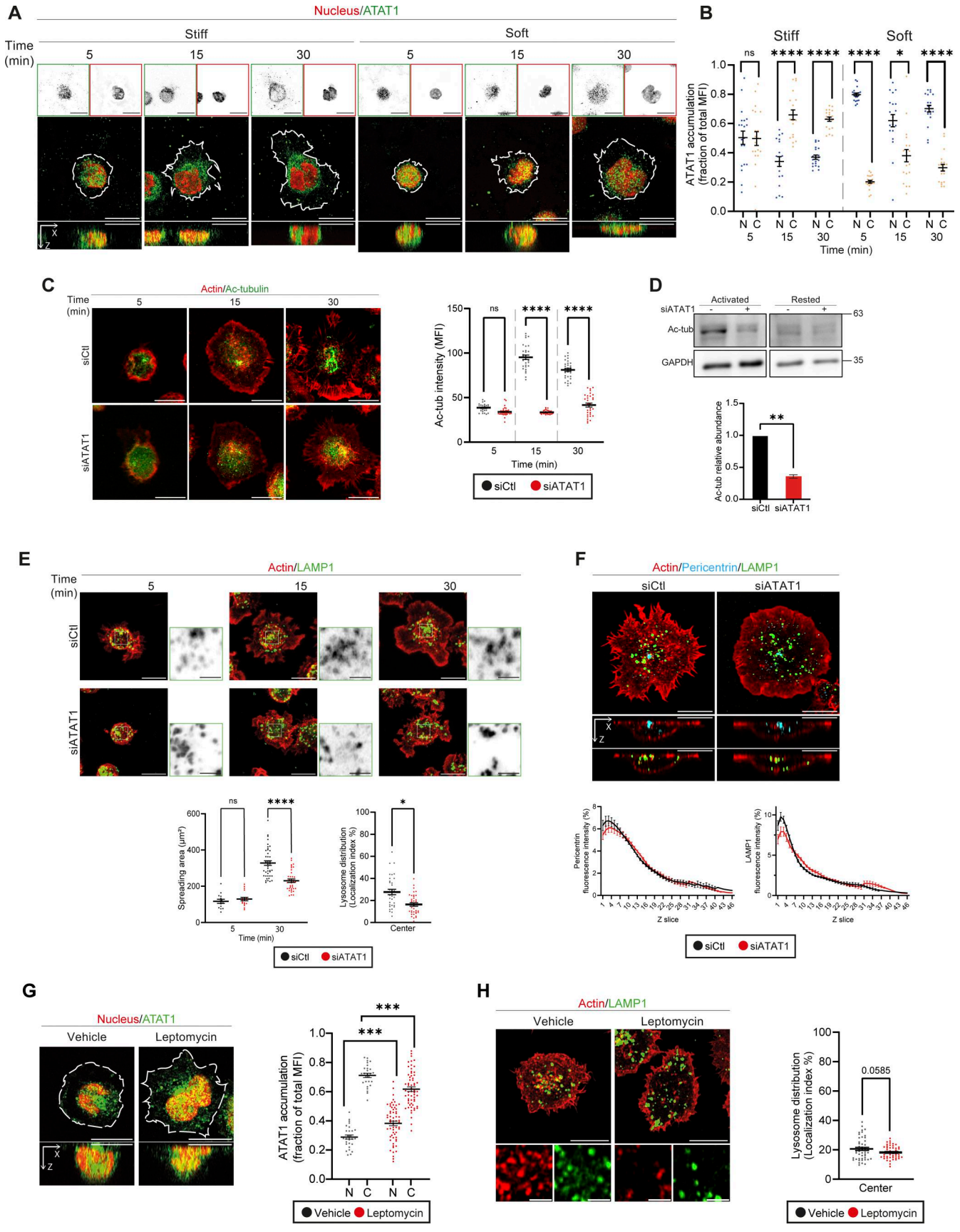

Figure 4. **Mechanotransduction regulates the localization of ATAT1 and controls lysosome positioning at the IS. (A)** Representative images of fixed B cells seeded on stiff or soft substrates containing BCR⁺ ligands for different time points. ATAT1 is shown in green, the nucleus in red (Hoechst), and the cell

border (white dashed outline) was defined by F-actin phalloidin staining. Scale bar: 10 µm. **(B)** Quantification of nuclear and cytoplasmic ATAT1 accumulation from the cells in A. The distribution index (y axis) represents the fraction of ATAT1 fluorescence in the nucleus (*N*, blue) or the cytoplasm (C, excluding the nucleus, gold) relative to the total cell area. **(C)** Representative images of control (siCTL) or ATAT1-silenced (siATAT1) B cells seeded on glass coverslips containing BCR$^+$ ligands for different time points. F-actin is shown in red, Ac-Tub is shown in green, and Ac-Tub density was calculated based on MFI at the IS for the images in C. **(D)** Western blot showing Ac-Tub and GAPDH from control or siATAT1 cells under activated (30 min) and resting conditions. Quantification is shown in the graph below. **(E and F)** Representative images of control (siCTL) or ATAT1-silenced (siATAT1) activated as in C. LAMP1 is shown in green, F- actin in red (phalloidin), and pericentrin (F) in cyan. Insets highlight the central pool of lysosomes, shown in grayscale. Graphs below show the quantification of cell spreading areas and LAMP1$^+$ lysosome accumulation at the IS center of B cells activated during 30 min, from cells represented in E. Z-scan profiles are shown from cells analyzed in F. **(G and H)** Representative images of B cells preincubated with vehicle (EtOH) or LMB and activated for 30 min on glass slides. In G ATAT1 is shown in green, the nucleus in red (Hoechst), and the cell border (white dashed outline), defined by actin staining. Graph shows ATAT1 density in the cytoplasm and nucleus, calculated based on MFI. **(H)** Cells were stained for LAMP1 and actin. Graph shows LAMP1$^+$ lysosome accumulation at the IS center of B cells activated during 30 min. Data consider $n \geq 30$ cells pooled from $N = 3$ independent experiments. Scale bars are 10 µm. Inset scale bars are 2 µm. **(B, C, and E)** (Right), G: Two-way ANOVA with Sidak's multiple comparison test. **(E)** (Left), H: *t* test. P values illustrated with asterisks are * <0.05, ** <0.01, *** <0.001, and **** <0.0001. Error bars are mean ± SEM. Source data are available for this figure: SourceData F4.

acetylation and lysosome distribution. We first validated ATAT1 silencing by assessing expression levels using immunofluorescence, as the ATAT1 antibody did not yield reliable results in western blot analysis. Immunofluorescence analysis showed that we were able to silence ATAT levels up to 50% of control cells (Fig. S4, A and B) independently of activating conditions.

Next, we evaluated the effect of ATAT1 silencing on tubulin acetylation. Considering that B cells activated on soft substrates display low levels of tubulin acetylation, we quantified MT acetylation in B cells activated on stiff substrates. To this end, control and siATAT1 B cells were activated on glass coverslips coated with BCR$^+$ ligands and stained for Ac-Tub. Indeed, ATAT1-silenced cells displayed lower levels of Ac-Tub compared with control cells during all times of activation (Fig. 4. C). Importantly, tubulin acetylation levels were rescued when expressing ATAT1-venus in siRNA ATAT1-silenced cells, excluding off-target effects (Fig. S4, C and D). We also performed western blot analysis of cell extracts from B cells seeded over stiff plastic plates coupled to BCR$^+$ or BCR$^-$ ligands (nonactivated) for 30 min. As expected, levels of Ac-Tub were dramatically reduced upon silencing of ATAT1 compared with control conditions (Fig. 4 D). Interestingly, cells activated over stiff substrates exhibited greater tubulin acetylation when in contact with BCR$^+$ ligands than in nonactivating conditions. These findings further support the role of the BCR in mechanotransduction, linking it to tubulin acetylation upon stimulation.

We next investigated the impact of ATAT1 silencing on lysosome positioning in B cells forming an IS. To this end, ATAT1-silenced and control B cells were seeded on glass coverslips and stained for LAMP1 and F-actin (Fig. 4 E). We analyzed both the cell spreading area and the distribution of lysosomes at the center of the IS. As anticipated, ATAT1-silenced B cells activated on stiff substrates failed to accumulate lysosomes preferentially at the IS center after 30 min, in contrast to control cells (Fig. 4 E). These cells also exhibited reduced spreading upon activation; however, centrosome repositioning to the synaptic membrane was unaffected (Fig. 4 F).

To further validate our findings, we determined whether perturbation of the nuclear export of ATAT1 affected MT acetylation in B cells. For this purpose, B cells were pretreated with 100 nM leptomycin B (LMB), an inhibitor of exportin-1–mediated nuclear export (Kudo et al., 1998), prior to activation on glass slides. Consistent with previous findings (Deb Roy et al., 2022), our results reveal that LMB treatment led to increased nuclear retention of ATAT1 compared with the vehicle control (Fig. 4 G), which was accompanied by a significant reduction in MT acetylation levels (Fig. S4 E). In agreement with these results, we observed that LMB-treated B cells activated on glass slides exhibited reduced lysosome recruitment to the center of the IS (Fig. 4 H), suggesting that impaired ATAT1 export from the nucleus hindered MT acetylation and lysosome recruitment to the synaptic membrane.

ATAT1 regulates the formation of actin foci at the IS of B cells

We next investigated the functional link between MT acetylation and actin foci formation in B cells during their response to mechanical cues. In other cell types undergoing adhesion and migration, both of which involve mechanotransduction, tubulin acetylation is enhanced, leading to the release of GEF-H1 from MTs into the cytoplasm. This process promotes Rho activity and increases cell contractility (Seetharaman et al., 2022). In B cells, GEF-H1 was identified as a key regulator in promoting the polarized polymerization of F-actin at the B cell synapse (Pineau et al., 2022). Our results show that both GEF-H1 and F-actin levels were significantly higher in B cells activated on stiff surfaces (Fig. S3,A and B). We therefore hypothesized that formation of actin foci, which relies on mechanotransduction, could be altered in ATAT1-silenced cells due to impaired MT acetylation and release of GEF-H1 to the IS. To this end, we first analyzed the levels of actin foci in control and ATAT1-silenced cells, stimulated on BCR$^+$ ligand–coated coverslips. Our results show that silencing ATAT1 reduces actin foci levels, preventing their accumulation at the center of the IS (Fig. 5 A). Notably, these cells also exhibited lower levels of GEF-H1 at the synaptic membrane, which failed to localize at the center of the synapse alongside actin foci, as observed in control cells (Fig. 5 B). Altogether, these findings suggest that B cell mechanotransduction depends on ATAT1, which enhances tubulin acetylation, thereby facilitating the accumulation of GEF-H1 at the synaptic membrane, where it regulates local actin polymerization.

Interestingly, we also observed that ATAT1-silenced B cells exhibited decreased pFAK levels at later time points of activation on stiff substrates (Fig. 5 C), supporting the interplay described between the formation of actin foci and tubulin

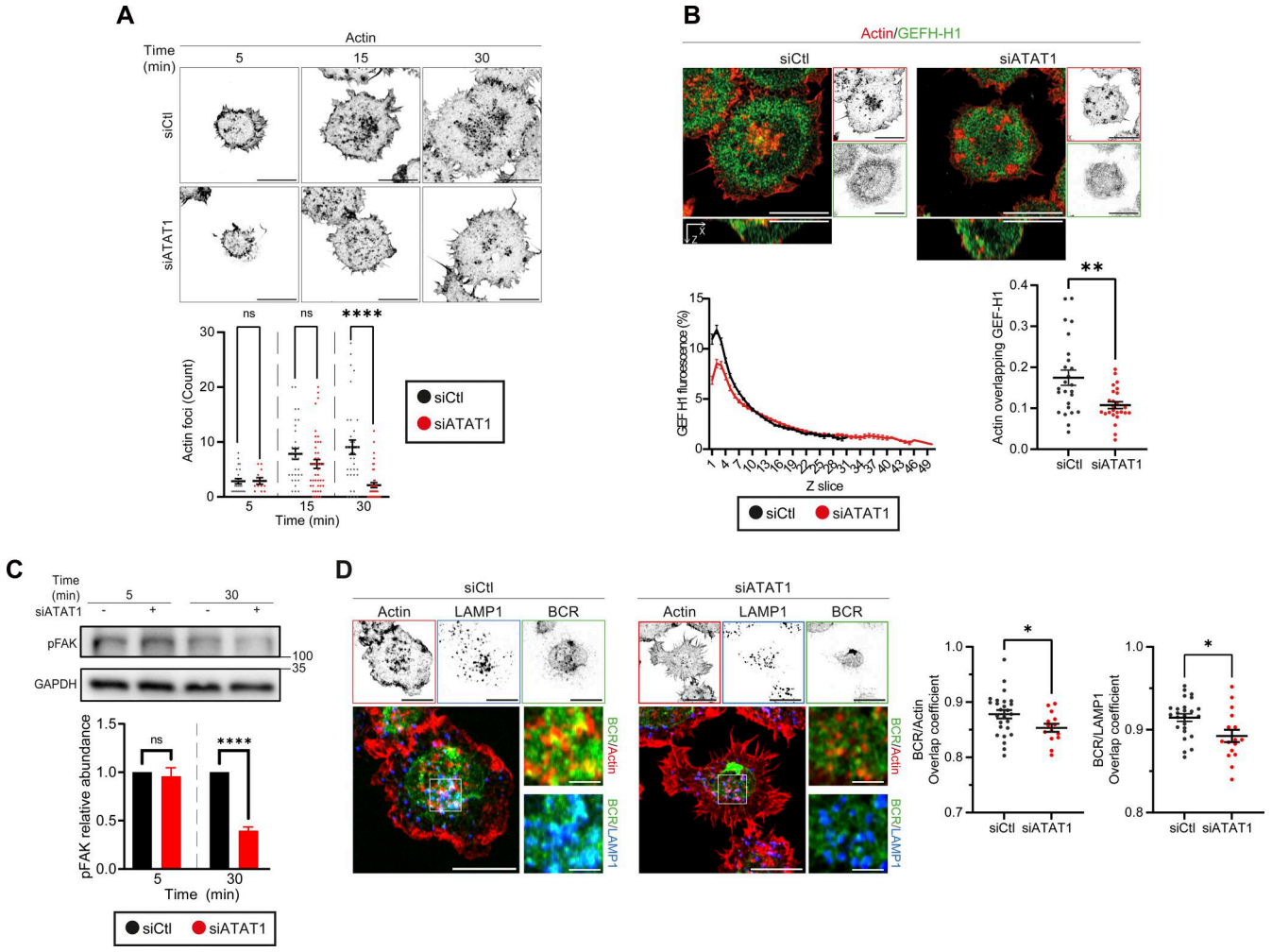

Figure 5. **ATAT1 regulates the formation of actin foci and organization of the BCR at the IS.** Representative images of control (siCTL) or ATAT1-silenced (siATAT1) B cells seeded on glass coverslips containing BCR⁺ ligands for different time points and stained for actin (grayscale). Quantification of actin foci at each time point shows a significant reduction in siATAT1 cells at 30 min (bottom panel). **(B)** Top: Representative images of control and ATAT1-silenced B cells seeded on glass coverslips containing BCR⁺ ligands activated for 30 min, stained for actin (red) and GEF-H1 (green). Lower panels: Z-scan fluorescence profile of GEF-H1 (left) and quantification of actin-GEF-H1 overlap revealing a significant reduction upon ATAT1 silencing (right). **(C)** Top: Western blot analysis of phosphorylated FAK (pFAK) at 5 and 30 min in siCTL and siATAT1 B cells. Bottom: Quantification shows a significant reduction in pFAK levels at 30 min in ATAT1-silenced cell. **(D)** Representative images of B cells stained for actin (red), lysosomes (LAMP1, blue), and the BCR (green) in siCTL and siATAT1 B cells activated for 30 min on glass coverslips containing BCR⁺ ligands. Graphs show quantification of BCR-actin and BCR-LAMP1 colocalization of images from D. Data consider $n \geq 30$ cells pooled from $N = 3$ independent experiments. Scale bars are 10 µm. Inset scale bars are 2 µm. **(A and C)**: Two-way ANOVA with Sidak's multiple comparison test. **(B and D)**: *t* test. P values illustrated with asterisks are * <0.05, ** <0.01, *** <0.001, and **** <0.0001. Error bars are mean ± SEM. Source data are available for this figure: SourceData F5.

acetylation. Such interactions could be a mechanism used by B cells to couple lysosome positioning to sites of antigen capture. Therefore, we next analyzed the localization of lysosomes and BCR at the IS in control and ATAT1-silenced cells. For this purpose, B cells were seeded on antigen-coated glass slides for 30 min and stained for LAMP1, actin, and the BCR. Notably, ATAT1-silenced cells displayed impaired synapse organization, where lysosomes, the BCR, and actin did not efficiently colocalize at the synaptic center compared with control cells (Fig. 5 D). Collectively, these results suggest that the MT acetylase, ATAT1, plays a critical role in the functional organization of the IS by positioning lysosomes and promoting the formation of actin foci where BCR-dependent antigen uptake occurs (Roper et al., 2019).

Mechanotransduction through ATAT1 regulates antigen extraction and presentation by B cells

Given that B cells rely on ATAT1 for actin foci formation and lysosome positioning at the IS, we next investigated whether this affects the extraction of immobilized antigens. To this end, we seeded control or ATAT1-silenced B cells expressing cathepsin-D-RFP on glass cover slips coupled with BCR⁺ ligand and the fluorogenic substrate DQ-OVA (DQ-ovalbumin) for 30 min. This substrate fluoresces upon cleavage by proteases, such as those present in lysosomes (Tang et al., 2023). After performing live-cell imaging using confocal microscopy (Fig. 6 A), we compared fluorescence intensities and radial distribution of the signal between both conditions. Our results show that control cells display higher fluorescence intensity associated with the

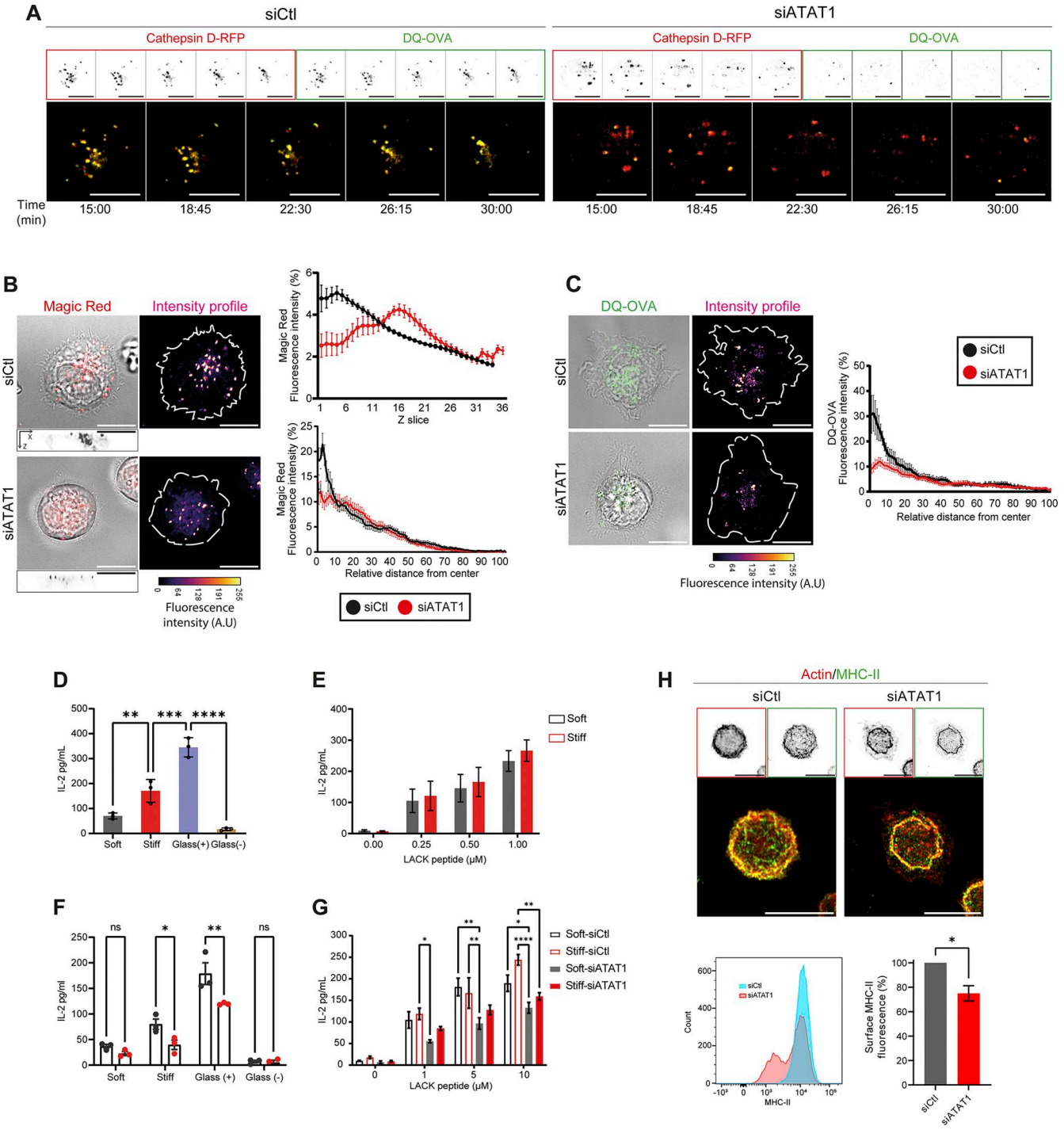

Figure 6. **ATAT1 is required for efficient antigen extraction and presentation by B cells. (A)** Time-lapse images of control (siCTL) or ATAT1-silenced (siATAT1) B cells expressing cathepsin D-RFP, activated on slides containing BCR$^+$ ligand plus DQ-OVA (green) during 30 min. Images show time points from 15 to 30 min. **(B and C)** siCTL and siATAT1 B cells activated for 30 min on BCR$^+$ ligand–DQ-OVA–coated slides. Representative images show MR and DQ-OVA staining at the synaptic interface, with corresponding fluorescence intensity maps. **(B)** Top graph: Quantification of MR fluorescence distribution in z-scan. **(B and C)** Radial distribution of fluorescence intensities according to their accumulation from the center to the periphery of the synapse plane. **(D–F)** Antigen presentation assays of B cells activated on substrates with different stiffness (D) and with control or ATAT1-silenced B cells (F). **(E and G)** Lack peptide control assays for the conditions shown. Mean amounts of IL-2 are shown for a representative of three independent experiments performed in triplicate. **(H)** Top: Representative immunofluorescence images of siCTL and siATAT1 cells stained for F-actin (red) and MHC-II (green). Bottom: Quantification of MHC-II at the cell surface by flow cytometry. Left: Representative histogram of MHC-II fluorescence intensity. Right: Quantification of MHC-II surface expression as a percentage relative to siCtl. Scale bars are 10 μm. Data consider $n \geq 30$ cells pooled from $N = 3$ independent experiments. **(D–G)** Two-way ANOVA with Sidak's multiple comparison test. **(H)**: t test. P values illustrated with asterisks are * <0.05, ** <0.01, *** <0.001, and **** <0.0001. Error bars are mean ± SEM.

degradation of surface-bound DQ-OVA concomitantly with an enhanced localization of the signal at the center of the IS (Fig. 6 A). Conversely, ATAT1- silenced cells degraded less antigen at the synaptic interface, as revealed by lower fluorescence levels of DQ-OVA across the cell, which did not accumulate at the center of the IS. Interestingly, these cells also exhibited a slightly reduced rate of soluble antigen uptake, most likely due to impaired actin organization (Fig. S5 B).

Next, we analyzed the localization of catalytically active lysosomes with the MR probe in B cells silenced or not for ATAT1. Here, each cell type was activated for 30 min on stiff glass substrates coupled with BCR^+ ligands, stained with MR, and imaged at the synaptic plane (Fig. 6 B). Our results show that ATAT1-silenced cells show a slight reduction in the accumulation of MR puncta at the synapse center within the inner center of the synapse compared with control cells (Fig. 6 C). Notably, ATAT1-silenced B cells displayed lower antigen extraction capacity as measured by the amount of fluorescent OVA at the synaptic interface (Fig. 6 C). Altogether, these results suggest that ATAT1 is required for the central positioning of catalytically active lysosomes at the synaptic membrane and is critical to promote the efficient extraction of immobilized antigens and could have an impact on their subsequent prestation on MHC class II (MHCII) molecules.

We next directly evaluated whether physical cues regulate the capacity of B cells to extract and present antigens, a fundamental step required for their complete activation. Our results show that B cells activated on stiff substrates displayed enhanced capacity to extract antigen from the synaptic interface (Fig. S5 A). We next decided to formally demonstrate if physical cues from the activating surface had an impact on the antigen presentation capacity of B cells. For this purpose, cells were activated over substrates of different stiffnesses containing specific BCR^+ ligands plus the LACK Ag from *Leishmania major*. Their ability to present LACK-derived MHCII–peptide complexes to a specific T cell hybridoma was then measured by monitoring interleukin-2 (IL-2) secretion. Importantly, we included a positive control for extreme stiffness (glass) coupled to BCR^+ or BCR^- ligands. As shown in Fig. 6 D, cells seeded on immobilized antigens associated to stiffer substrates, triggered higher IL-2 production from T cells in comparison with B cells activated on soft substrates. This suggests a positive correlation between substrate stiffness and the capacity of B cells to extract, process, and present antigens to T cells. Increasing levels of stiffness had no effect on the presentation of the $LACK_{156–173}$ peptide, showing that varying substrate rigidity does not significantly influence T cell responses or B–T cell interactions (Fig. 6 E).

Having shown that physical cues from the environment regulate the capacity of B cells to extract and present immobilized antigens, we next evaluated whether this relied on ATAT1-dependent MT acetylation. For this purpose, B cells were silenced for ATAT1, and their capacity to extract and present antigens was assessed using the previously described experimental setup. As shown in Fig. 6 F, the capacity to present Lack antigen associated to stiff substrates was lower in ATAT1-silenced B cells compared with controls cells. However, no significant differences between control and ATAT1-silenced cells were observed when activated on soft substrates. This result is consistent with our observations showing that B cells activated on soft substrates display low levels ATAT1 translocation to the cytoplasm and MT acetylation, and therefore silencing of this enzyme should not have a major effect on antigen presentation. Additionally, the capacity of ATAT1-silenced B cells to present processed $LACK_{156–173}$ peptide was lower compared with control cells (Fig. 6 G), suggesting that B–T cell interactions or that trafficking of MHCII molecules to the cell surface could be affected. To evaluate this, surface levels of MHCII were measured by immunofluorescence staining and flow cytometry in control and ATAT1-silenced B cells and (Fig. 6 H). Our results reveal that, indeed, B cells silenced for ATAT1 display lower levels of MHCII on the surface compared with control counterparts, indicating that MHCII trafficking to the cell surface relies on ATAT1. Collectively, these results suggest that silencing ATAT1 compromises the capacity of B cells to enhance antigen extraction and presentation. Such defects likely result from defective mechanotransduction pathways, impairing the formation of actin foci and MT acetylation, which lead to disrupted cytoskeletal dynamics, thereby compromising the transport of MHCII-containing vesicles to the plasma membrane.

Discussion

Immune cells both sense and exert mechanical forces at cell–cell interfaces, shaping signal transduction and intercellular communication at the IS (Basu et al., 2016; Basu and Huse, 2017; Friedman et al., 2021). Consequently, lymphocyte activation is a mechanically regulated process, in which cytoskeletal forces modulate immune receptor clustering and downstream signaling cascades (Pathni et al., 2024; Rogers et al., 2024). This study uncovers a mechanotransduction pathway in B lymphocytes that coordinates lysosome trafficking and cytoskeletal remodeling as interconnected processes, enabling B cells to integrate physical cues and fine-tune their ability to extract and present antigens.

Our study shows that B cells activated on stiffer surfaces exhibit canonical mechanotransduction responses, including nuclear translocation of YAP, actin foci formation, and activation of FAK, indicating that they respond to mechanical stimuli and are efficiently activated under these conditions. Actin foci are highly dynamic actin structures that play a central role in antigen recognition and BCR signaling regulation. Their formation and function are N-WASP and Arp2/3 dependent and provide anchor points for myosin II, helping form contractile actomyosin arcs, which regulate the movement of BCR clusters and control receptor organization (Roper et al., 2019). Importantly, actin foci have been shown to serve as sites where antigen is concentrated and acquired and could explain why B cells activated on stiff surfaces exhibit enhanced capacity to capture antigens (Roper et al., 2019).

Our data reveal that B cells activated on stiffer substrates display increased levels of acetylated MTs, which progressively accumulate over time. Whether B cell activation in response to stiffness also induces other PTMs of tubulin—such as tyrosination, glutamylation, or phosphorylation—remains to be

explored. Notably, we observed increased accumulation of GEF-H1 at the IS in B cells activated on stiffer substrates, a process dependent on the acetylase, ATAT1. In this context, recent studies in B lymphocytes have shown that the release and activation of GEF-H1 by MTs at the IS helps to focus F-actin polymerization, thereby promoting proteolytic extraction of antigens at one unique site (Pineau et al., 2022). In agreement with this notion, B cells silenced for ATAT1 also display fewer actin foci, which remain dispersed at synaptic interface, similarly to observations made in GEF-H1-silenced cells (Pineau et al., 2022). ATAT1-silenced B cells also have decreased levels of activated FAK (phospho-FAK), suggesting that acetylation of MTs helps stabilize actin foci, analogously to observations made in focal adhesions, where MT acetylation is crucial for focal adhesion stability and turnover at the leading edge of migrating cells (Bance et al., 2019). However, other studies have shown that physical cues perceived by $CD8^+$ T cells trigger the activation of WASP, which drives actin foci formation and enhances their activation and cytotoxic capacity (Mandal et al., 2023). Thus, we cannot exclude that in B cells, actin foci formation coupled to mechanotransduction might also result from the activation of WASP and occur independently of MT acetylation and GEF-H1.

We previously showed that GEF-H1 is critical for the correct assembly of the exocyst complex, which enables lysosome tethering at the center of the IS to promote the efficient extraction and processing of immobilized antigens (Sáez et al., 2019). Lysosome clustering at the center of the IS, previously described as a secretory domain in other lymphocytes (Wang et al., 2022), could also facilitate antigen extraction in addition to the processing of incoming antigens. Thus, mechanotransduction pathways leading to enhanced MT acetylation are coupled to lysosome trafficking as well as actin cytoskeletal remodeling at the synaptic interface, which could reinforce this specialized domain dedicated to antigen extraction and processing. Other studies in neutrophils have shown that GEF-H1 deficiency results in impaired migration and recruitment to inflamed tissues, along with defects in actin dynamics (Fine et al., 2016). Similarly, in B cells, mechanical cues could also influence cellular functions, such as directed migration, which is essential for recruiting T cell help and establishing a robust immune response (Carrasco and Batista, 2007; Maiuri et al., 2015).

The association of lysosomes with acetylated MTs was observed in other polarized cell types but not previously demonstrated in B cells. Kinesin motor proteins, such as KIF1 and KIF5, likely mediate this association by promoting selective lysosome binding to acetylated MTs (Bhuwania et al., 2014; Serra-Marques et al., 2020; Dunn et al., 2008). However, the direct involvement of these motor proteins in B cells remains to be determined. Interestingly, inhibiting HDAC6, which enhances tubulin acetylation, did not affect lysosome dynamics in B cells activated on stiff substrates. This suggests the existence of an "acetylation threshold" that fine-tunes lysosome positioning at the IS. Conversely, ATAT1-silenced B cells exhibited fewer lysosomes with high proteolytic activity at the IS center, even under stiff conditions. This finding supports our model in which tubulin acetylation functions as a regulatory node, ensuring that lysosomes are properly positioned at the secretory domain of the IS to optimize antigen extraction and processing. However, the molecular machinery linking antigen-processing compartments to acetylated MTs remains to be elucidated.

ATAT1 is the only known enzyme responsible for catalyzing tubulin acetylation and has recently been shown to shuttle between the nucleus and cytoplasm, modifying tubulin lattices (Deb Roy et al., 2022; Even et al., 2019). Our results show that with increasing activation time and substrate stiffness, ATAT1 progressively relocates from the nucleus to the cytoplasm in B cells. The mechanism by which mechanical cues regulate this trafficking remains unclear. One possibility is that the LINC complex, which connects integrin signaling with nuclear architecture, mediates nuclear pore opening in response to mechanical stimuli (Takata and Matsumura, 2022; Bouzid et al., 2019). Importantly, the LINC complex plays a crucial role in B cells by promoting nuclear and MT-organizing center reorientation at the IS (Ulloa et al., 2022). We propose that mechanical cues from stiff substrates induce nuclear pore opening, allowing ATAT1 to translocate to the cytoplasm, where it facilitates tubulin acetylation in response to BCR stimulation.

A critical step in B cell activation is the presentation of antigens as peptide fragments on MHCII molecules to T cells, enabling B–T cell cooperation and supporting B cell maturation into plasma cells (Akkaya et al., 2020). Our experiments demonstrate that B cells exposed to antigens immobilized on stiff substrates elicit increased IL-2 secretion from T cells, highlighting the role of BCR-mediated mechanotransduction in upregulating the capacity to extract and present immobilized antigens. However, substrate stiffness did not significantly affect the presentation of the LACK peptide, suggesting minimal impact on overall B–T cell interactions. As highlighted by Trappmann et al. (2012), the mechanical properties of the substrate can influence ligand tethering and availability. Thus, we cannot rule out that co-stimulation resulting from serum-derived adhesion molecules on stiff versus soft hydrogels could also account for the defective spreading of B cells observed in the latter. In this sense, future experiments, including adhesion molecules on soft gels, could be used to compensate for this spreading defect, enabling to discriminate between mechanoresponses and biochemical-dependent adhesion. Interestingly, ICAM-1 has been shown to facilitate the formation of actomyosin contractile arcs at the B cell synapse, thereby enhancing adhesion and mechanical stability (Wang et al., 2022). Future studies should focus on elucidating the role of integrin-mediated co-stimulation, particularly via ICAM-1, in B cell mechanotransduction. Understanding its mechanistic contribution could provide deeper insights into the biomechanical regulation of B cell activation.

Notably, B cells lacking ATAT1 exhibited slightly reduced uptake of soluble BCR ligands, potentially due to impaired actin remodeling, which is known to play a key role in BCR endocytosis (Liu et al., 2013; Cabrera-Reyes et al., 2024). Interestingly, ATAT1 has been shown to interact with AP2, suggesting that clathrin-coated pits may regulate tubulin acetylation—an interplay that could, in turn, influence BCR internalization rates (Montagnac et al., 2013). Furthermore, B cells silenced for ATAT1 displayed a reduced capacity to extract and present immobilized

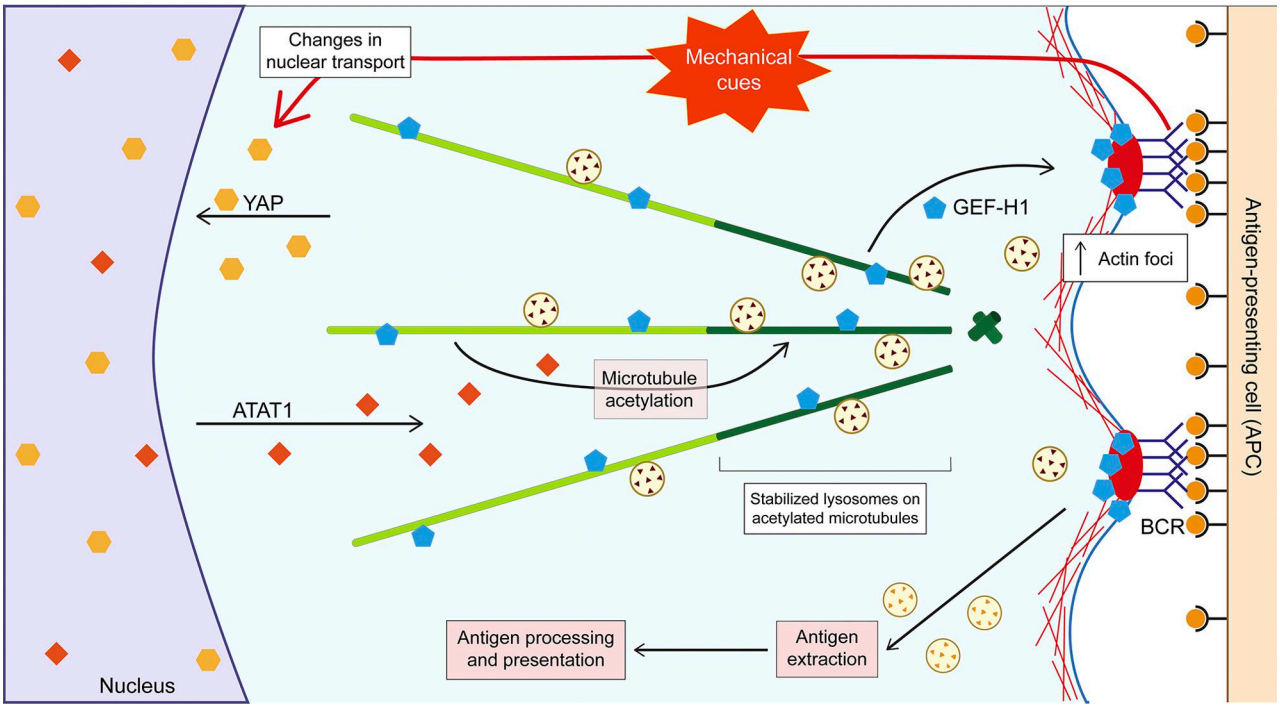

Figure 7. **Schematic representation of the mechanotransduction pathway that enables B cells to extract and present immobilized antigens.** B cells sense substrate stiffness by the BCR, leading to the nuclear translocation of YAP 1 and the export of the ATAT1 to the cytoplasm. This results in increased MT acetylation, facilitating the release of GEF-H1 at the IS, which in turn promotes actin foci formation. Simultaneously, acetylated MTs serve as stabilized tracks for lysosome positioning at the IS, thereby enhancing antigen extraction and presentation.

antigens to T cells compared with controls. However, no significant differences in IL-2 production were observed in antigen presentation assays using B cells activated on softer substrates. It is possible that soft environments do not sufficiently promote ATAT1 translocation to the cytoplasm, which could explain why functional outcomes remained similar regardless of ATAT1 expression under these conditions. Our assay also revealed that B cells silenced for ATAT1 displayed reduced presentation capacity of LACK peptides, suggesting that B–T cell interactions were affected. Supporting this, surface levels of MHCII were significantly lower in ATAT1-silenced cells compared with controls, indicating that ATAT1 may regulate MHCII trafficking, most likely through its role in maintaining MT stability (Rocha and Neefjes, 2008). Interestingly, mechanical cues were recently shown to influence the remodeling and redistribution of the ER toward the IS (Riobó and Yuseff, 2024). How this is coupled to antigen processing and presentation, however, remains to be elucidated.

In summary, our findings highlight how B cells integrate mechanical cues to regulate lysosome dynamics and optimize antigen extraction through the formation of actin foci (Fig. 7). Elucidating this pathway could advance strategies for vaccine development, targeted drug delivery, and therapeutic interventions for autoimmune diseases.

Materials and methods

Cell lines, culture, and treatments

In this study, we used the murine A20 B lymphoma cell line, which exhibits a phenotype consistent with quiescent mature B cells, and the LMR7.5 T cell hybridoma, a $CD4^+$ T cell line that specifically recognizes I-A^d–LACK peptide–MHCII complexes. Both cell lines were maintained at 37°C in a humidified incubator with 5% CO_2 and CLICK medium, consisting of RPMI 1640 with GlutaMAX (Gibco) supplemented with 10% heat-inactivated FBS (Gibco), 0.1% 2-mercaptoethanol (Gibco), 100 U/ml penicillin, 100 µg/ml streptomycin (Gibco), and 1 mM sodium pyruvate (Gibco).

To induce tubulin acetylation, cells were treated for 30 min with 1 µM of SAHA, a histone deacetylase inhibitor (#149647-78-9; Tocris Bioscience), prior to activation or downstream experimental procedures. For inhibition of nuclear export, cells were incubated for 3 h with 20 nM Leptomycin B (#L2913; Sigma-Aldrich).

Preparation of tunable-stiffness PAA gels

For preparing the tunable-stiffness PAA gels, two sets of coverslips are used: a silanized-bottom coverslip, where the PAA gel is immobilized, and a smaller impermeabilized coverslip on top to create a "sandwich" to allow for the polymerization of the PAA gel (Charrier et al., 2020). Bottom coverslips are activated with a 2% 3-Aminopropyltrimethoxysilane (13822-56-5; Sigma-Aldrich) in 96% ethanol solution for 5 min and washed with 70% ethanol. The top coverslips are siliconized or waterproofed with Rain-X. The coverslips are then washed with ultrapure water, dried well, and moved to the next stage.

The following reagents were used to prepare 0.3 and 13-kPa PAA gels: 2% bis solution (#1610142; Bio-Rad), 40% acrylamide (#1610140; Bio-Rad), 10% APS in 10 mM HEPES solution, and

TEMED. To prepare a 0.3-kPa gel, the following components were mixed to achieve a total volume of 1,011 µl: 75 µl of 40% acrylamide (constituting ∼7.42% of the total volume), 30 µl of 2% bis-acrylamide (∼2.97%), 10 µl of 10% APS (∼0.99%), 1 µl of TEMED (∼0.10%), and 895 µl of 1X PBS (∼88.52%). The proportions of the components are as follows: acrylamide to bis-acrylamide at a ratio of 2.5:1, acrylamide to APS at a ratio of 7.5:1, acrylamide to TEMED at a ratio of 75:1, and acrylamide to PBS at a ratio of ∼1:12.

For the 13-kPa gel, the components were combined to a final volume of 1,249 µl as follows: 233.75 µl of 40% acrylamide (∼18.71%), 125 µl of 2% bis-acrylamide (∼10.01%), 6.25 µl of 10% APS (∼0.50%), 1.8 µl of TEMED (∼0.14%), and 883 µl of 1X PBS (∼70.64%). The proportions of the components are as follows: acrylamide to bis-acrylamide at a ratio of ∼1.87:1, acrylamide to APS at a ratio of ∼37:1, acrylamide to TEMED at a ratio of ∼130:1, and acrylamide to PBS at a ratio of ∼1:4.

To prepare the gel, 9 µl of the gel solution was pipetted onto the center of the bottom coverslip. Then, it was covered with the smaller cover and pressed gently until the mix spread outward. After 30 min of polymerization, PBS was added to carefully remove the top cover. The gel was stored in fresh PBS at 4°C overnight and used within 48 h.

For conjugation with ligands, a solution of 0.5 mg/ml sulfo-SANPAH (#A35395; Pierce; Thermo Fisher Scientific) in HEPES buffer 10 mM was prepared. PBS was removed from the gels and immediately coated with sulfo-SANPAH at RT. Gels were exposed to 365-nm UV light (Maestrogen UV illuminator MLB-16) for 10 min and washed with 1X PBS thrice. Finally, a BCR^+ ligand (F(ab′)2 goat anti-mouse IgG) (115-006-146; Jackson ImmunoResearch) was added to coat the gels at a concentration of 0.13 mg/ml and incubated overnight. This was followed by three washes with 1X PBS and immediately used for experiments or stored at 4°C protected from light for no more than 48 h.

Activation and immunofluorescence of B cells on PAA gels

80 µl of B cells (1.0×10^6 cells/ml in CLICK medium with 5% FBS) were seeded onto an antigen (BCR ligand$^+$)-coated gel for different time points in a cell incubator at 37°C/5% CO_2. After each time point, the media was carefully aspirated off each PAA gel, and 100 µl of cold 1X PBS was added to stop the activation. PBS was removed, and each PAA gel was fixed with 50 µl of 3% PFA for 10 min at RT. PAA gels were washed three times with 1X PBS. The 1X PBS was removed, and 50 µl of blocking buffer (2% BSA and 0.3 M glycine in 1X PBS) was added to each coverslip.

Primary antibodies were diluted in permeabilization buffer (0.2% BSA and 0.05% saponin in PBS) and incubated by adding 40 µl over the gels in a humid chamber at 4°C overnight. The plate was sealed to avoid evaporation of the antigen solution. Gels were washed three times with permeabilization buffer. Secondary antibodies or dyes were diluted in permeabilization buffer, using 40 µl per PAA gel, and incubated for 1 h at RT in dark and humid chambers. The PAA gels were washed twice with permeabilization buffer and once with 1X PBS. The PBS solution was removed from the coverslips. 8 µl of mounting reagent was added to a microscope slide. The PAA gels were mounted onto the slide with the cell side facing down. The slides were allowed to dry for 30 min at 37°C or RT overnight protected from light.

Immunoblot

Cells were lysed with 40 µl of RIPA buffer, then supernatants of samples were collected and loaded onto gels and transferred onto polyvinylidene fluoride membrane (Trans-Blot Semi-Dry Transfer Cell; Bio-Rad). Membranes were blocked in 2% BSA/TBS + 0.05% Tween-20 and incubated overnight at 4°C with primary antibodies, followed by 60-min incubation with secondary antibodies. Western blots were developed with Westar Supernova substrate (Cat. No. XLS3,0100; Cyanagen), and chemiluminescence was detected using the iBright imager (Thermo Fisher Scientific).

AFM

The elastic modulus of the PAA gels (Young's modulus, E) was assessed using a JPK NanoWizard with a CellHesion module mounted on a Carl Zeiss confocal microscope, Zeiss LSM510 (AFM; JPK instruments), and silicon nitride cantilevers (spring constant: 1 Nm^{-1}, spherical 10-µm diameter tip; Novascan Technologies).

Force measurements were conducted at different locations (0.5-mm apart in x and y coordinates) within the region of interest. In each location, nine indentations distributed in a 3 × 3 point grid (30 × 30 µm) were performed. The elastic modulus for each force curve was calculated using JPK data processing software (JPK DP version 4.2), assuming a Hertz impact model.

Antibodies and dyes

The following primary antibodies were used for immunofluorescence: rat monoclonal anti-mouse LAMP1 (clone 1D4B; #553792; RRID: AB_2134499; 1:200; BD Biosciences), rabbit monoclonal anti-acetylated α-tubulin (Lys40, clone D20G3; #5335; RRID: AB_10544694; 1:200; Cell Signaling Technology), rabbit polyclonal anti-mouse α-tubulin (#ab6160; RRID: AB_305328; 1:500; Abcam), goat polyclonal anti-mouse IgM $F(ab')_2$ (#115-006-075; RRID: not available; Jackson ImmunoResearch), rabbit polyclonal anti-mouse GEF-H1 (#ab155785; RRID: AB_10679354; 1:200; Abcam), rat monoclonal anti-mouse MHC class II (clone NIMR-4; #ab25333; RRID: AB_778167; 1:200; Abcam), rabbit polyclonal anti-mouse ATAT1 (#PA5-114922; RRID: not available; 1:200; Thermo Fisher Scientific), and rabbit monoclonal anti-mouse YAP (clone D8H1X XP; #14074; RRID: AB_2650491; 1:200; Cell Signaling Technology).

Secondary antibodies included donkey $F(ab')_2$ anti-rabbit IgG conjugated to Alexa Fluor 488, 546, or 647 (#711-546-152; RRID: AB_2340619; 1:200; Jackson ImmunoResearch), and donkey $F(ab')_2$ anti-rat IgG conjugated to Alexa Fluor 488, 546, or 647 (#712-166-153; RRID: AB_2340669; 1:200; Jackson ImmunoResearch). F-actin was visualized using rhodamine-conjugated phalloidin (R415; RRID: AB_2572408; 1:200; Thermo Fisher Scientific). Lysosomes were labeled with LysoTracker Red DND-99 (#L7528; 50–100 nM; Thermo Fisher Scientific). Nuclei were counterstained with Hoechst 33342 (ab228551; 1 µg/ml; Abcam).

For functional assays, DQ-OVA (#D12053; Thermo Fisher Scientific) was used to monitor antigen degradation, and Magic

Red (#ICT937; ImmunoChemistry Technologies) was used to detect lysosomal cathepsin B activity in live cells, following the manufacturers' instructions.

Cell transfection and plasmids

Electroporation was performed using the Nucleofector R T16 device (Lonza). A total of 4 × 10^6 A20 B cells were electroporated with 3 µg of plasmid DNA using the LC-013 pulse program, according to the manufacturer's instructions. After transfection, cells were cultured in CLICK medium at 37°C with 5% CO_2 for 18 h prior to functional analysis.

For gene silencing of ATAT1, cells were electroporated with 100 nM of either a mouse-specific siRNA-targeting ATAT1 (#sc-108799-SH; Santa Cruz Biotechnology) or a non-targeting control siRNA (#sc-37007; Santa Cruz Biotechnology). All siRNA reagents were delivered under the same electroporation conditions described above.

The mVenus–ATAT1 expression plasmid used for ectopic expression experiments was kindly provided by Dr. A. Deb Roy (Johns Hopkins Medical Institute, Baltimore, MD, USA). This construct encodes a fusion protein consisting of the mouse ATAT1 gene tagged at the N terminus with the fluorescent protein mVenus.

Antigen extraction and lysosome activity using DQ-OVA and MR

For antigen extraction assays, cells were incubated with DQ-OVA (D12053; Thermo Fisher Scientific) at a concentration of 0.13 mg/ml. This probe was coupled to glass coverslips or PAA gels in combination with BCR ligands for 1 h at room temperature. Lysosomal activity was assessed using Magic Red (ICT937; ImmunoChemistry Technologies), following the manufacturer's protocol. Cells were incubated with the probe for 20 min, then seeded onto antigen-coated substrates. After 15 min of incubation at 37°C, cells were imaged by confocal microscopy for an additional 15 min. Images were acquired using a Zeiss LSM 880 confocal microscope with Airyscan detection (Carl Zeiss Microscopy GmbH), equipped with a Plan-Apochromat 63×/1.4 NA oil-immersion objective. Cells were maintained at 37°C in a temperature-controlled chamber during live imaging. The imaging medium consisted of phenol red-free RPMI supplemented with 10% FBS. Fluorophores used in these assays included DQ-OVA (green fluorescence) and MR (red fluorescence).

Images were captured using a GaAsP 32-channel Airyscan detector and the ZEN Black software (version 2.3; Zeiss). Airyscan processing and joint deconvolution were performed within ZEN. Postprocessing steps, such as brightness and contrast adjustment, were applied linearly using Fiji/ImageJ.

Antigen presentation assay

Antigen presentation assays were performed as described by Yuseff et al. (2011) with modifications. Briefly, B cells were seeded on PAA gels coated with either Lack protein plus BCR-ligand or BCR ligand alone in the presence of different concentrations of soluble Lack peptide (156-173; Lack) for 2 h. Then, cells were washed with PBS and fixed with ice-cold 0.01% glutaraldehyde for 30 s. After fixation, cells were washed and incubated with Lack-specific LMR 24 7.5 T cells in a 1:2 ratio for overnight at 37°C and 5% CO_2. Supernatants were collected, and IL-2 cytokine production was measured using BD optiEA Mouse IL-2 ELISA set following the manufacturer's instructions (cat no. 555148; BD Biosciences).

Measurement of antigen-BCR internalization and MHCII surface levels by flow cytometry

Antigen internalization

Control and ATAT1-silenced B cells (5 × 10^5) were washed once with PBS and then resuspended in internalization buffer (RPMI 1640, 5% FCS, 10 mM glutamine, 5 mM sodium pyruvate, 50 mM 2-ME, and 10 mM HEPES, pH 7.4) at a density of 5 × 10^6 cells/ml. Next, cells were incubated with 10 µg/ml F(ab′)$_2$ goat anti-mouse IgG premixed to 20 µg/ml donkey anti-goat IgG for 30 min on ice. Cells were then washed with ice-cold PBS/2% serum to remove the excess ligand and incubated at 37°C for 0–30 min. Internalization was stopped by incubating the cells on ice and adding ice-cold PBS/2% serum. To detect BCR remaining on the cell surface, cells were stained on ice with anti-mouse BCR-Alexa 488, washed twice with PBS plus 3% BSA, and fixed with 1% PFA. Flow cytometry was performed using a FACS Canto II cytometer, and mean fluorescence intensity was analyzed with FlowJo software (BD Biosciences). The percent of BCR on the cell surface was calculated as (MFI at 37°C)/(MFI at 4°C) × 100.

Cell surface MHCII levels

Control and ATAT-silenced B cells (5 × 10^5) cells were incubated on ice for 20 min and stained with anti-mouse MHCII-Alexa 647, washed with ice-cold PBS/2% serum, and fixed with 1% PFA. Cells were washed, and flow cytometry was performed using a FACS Canto II cytometer. Data were analyzed for mean fluorescence intensity with FlowJo software (BD Biosciences).

Cell imaging and analysis

For widefield imaging, Z-stacks were acquired with 0.3-µm axial spacing using a Nikon Eclipse Ti inverted epifluorescence microscope equipped with a Plan Fluor 60×/1.25 NA oil-immersion objective and an iXon Ultra EMCCD camera (Andor Technology). Image acquisition was performed using NIS-Elements Advanced Research software (Nikon Instruments). For confocal microscopy, images were acquired using a Zeiss LSM 880 microscope with Airyscan detection (Carl Zeiss Microscopy GmbH), equipped with a Plan-Apochromat 63×/1.4 NA oil-immersion objective. Z-stacks were collected using an axial step size of 0.2 µm. All image acquisition across experimental replicates was conducted under identical illumination conditions, maintaining constant laser power (mW/cm^2) or exposure times. Airyscan images were processed using ZEN Black software (Zeiss) with standard Airyscan deconvolution settings. Postprocessing and quantification were performed in Fiji/ImageJ (Schindelin et al., 2012).

To analyze cell spreading, maximum intensity projections of F-actin staining were first thresholded using the Otsu algorithm to generate binary masks. When automatic segmentation failed to accurately capture the boundaries of spreading cells—particularly

in images with heterogeneous actin intensity—manual correction was performed using the freehand selection tool in Fiji (ImageJ). Only well-defined spreading cells with a continuous actin ring and central F-actin clearance were included in the analysis. Actin foci were quantified by applying a secondary threshold within the previously segmented spreading area. A band-pass filter (using the "Subtract Background" and "Gaussian Blur" tools) was applied to enhance discrete punctate structures. Particle analysis was then performed using Fiji's "Analyze Particles" function, with a size threshold of 0.1–1.5 μm^2 and circularity range of 0.3–1.0 to exclude noise and elongated structures. Lysosome dynamics were analyzed using the TrackMate plugin in Fiji, employing the LAP tracker with default unsupervised settings, and validating tracks based on quality scores. Colocalization and fluorescence intensity ratios were determined by quantifying the mean fluorescence intensity of segmented structures in single z-planes corresponding to the IS plane, defined as the optical section closest to the PAA gel surface. Colocalization analysis was performed on single planes and individual regions of interest using the JaCoP plugin in Fiji according to its documentation.

To assess lysosome positioning within activated B cells, a localization index was calculated by quantifying the distribution of lysosomal fluorescence between central and peripheral regions of the cell. The total cell area was first segmented manually based on F-actin staining, and the centroid of the nucleus—identified via Hoechst 33342 staining—was used as a reference point to define a central region encompassing 50% of the cell radius. Fluorescence intensity from lysosomal markers, such as LAMP1 or LysoTracker, was measured within this central region and across the entire cell. The localization index was then defined as the ratio of central fluorescence to total fluorescence intensity, where values close to one indicate a perinuclear accumulation of lysosomes, while lower values reflect a peripheral redistribution (Ibañez-Vega et al., 2019b).

To quantify nuclear versus cytoplasmic distribution of fluorescent signals, the Cyt/Nuc plugin in Fiji (ImageJ) was used (Grune et al., 2018). Nuclei were segmented using Hoechst staining, and cytoplasmic regions were defined by subtracting the nuclear mask from the total cell area previously segmented based on F-actin boundaries. Mean fluorescence intensities for each marker of interest, such as ATAT1 or YAP, were measured separately within the nuclear and cytoplasmic compartments. A cytoplasmic-to-nuclear ratio was calculated for each individual cell to determine the relative distribution of the protein or signal between these compartments. For fluorescence distribution across the z-stack, a custom macro in Fiji and an R script were used to measure the raw fluorescence in each z-slice, and values were expressed as a percentage of the total cell fluorescence. Scripts and macros are publicly available at https://github.com/YuseffLab/Z-stack-multimeasure.

Finally, radial distribution analysis of DQ-OVA and MR was performed using a custom macro in Fiji that implements the eroded volume fraction method to normalize fluorescence intensity relative to distance from the cell center toward the periphery.

Statistical analysis

All data presented were tested for normality and homoscedasticity; accordingly, appropriate statistical tests were applied considering those factors. Data in plots and graphs are expressed as fold change of mean or mean ± SEM. If corresponding, experiments were analyzed by Student's *t* test or Mann–Whitney test following Gaussian and non-Gaussian distribution, respectively, after performing d'Agostino and Pearson omnibus normality test. In cases where two conditions are shown, two-way ANOVA with Sidak's multiple comparison test was performed if data followed normal distribution. When datasets followed non-Gaussian distributions, Kruskal–Wallis tests were applied with Dunn's a posteriori multi-comparison examination. Experiments were carried out with a sum of $n \geq 30$ cells pooled from $N = 3$ biological replicates. Error bars shown are mean ± SEM. Statistical analysis was performed with Prism (GraphPad Software) and RStudio. For significance, P values were calculated using different tests mentioned above and are illustrated in each figure.

Online supplemental material

Fig. S1 shows the basic workflow used to activate B cells on PAA gels and AFM measurements in kPA of gel stiffness. Fig. S2 shows the western blot analysis of downstream BCR signaling molecules or levels of Ac-Tub in B cells activated on soft and stiff surfaces for different time points. Fig. S3 contains the immunofluorescent staining for GEF-H1, actin, Lamp1, or α-Tub in B cells activated on soft or stiff substrates and corresponding quantifications. Fig. S4 shows the levels of ATAT1 in control or ATAT1-silenced B cells and Ac-Tub levels in ATAT1-silenced B cells expressing ATAT1-venus or empty vector or upon treatment with LMB. Fig. S5 shows the time-lapse images of control or ATAT1-silenced B cells expressing cathepsin D-RFP, activated on soft or stiff substrates coated with BCR^+ ligands plus DQ-OVA (green) to monitor antigen extraction and BCR endocytosis rates in siCtl and siATAT1 B cells measured by flow cytometry. Video 1 shows the cathepsin D-RFP–expressing B cells activated on soft or stiff substrates. Video 2 shows the B cells expressing cathepsin D-RFP, activated on soft or stiff substrates treated or not with the histone deacetylase inhibitor (SAHA).

Data availability

All data supporting the findings of this study are available within the article and its supplementary information files. Uncropped western blots are included in the Source Data. Custom analysis scripts are available at our GitHub repository: https://github.com/YuseffLab. Additional materials are available from the corresponding author upon reasonable request.

Acknowledgments

We thank the Unidad de Microscopía Avanzada from Pontificia Universidad Católica de Chile, especially Nicole Salgado and Fernanda Gárate, for their support in image acquisition.

This work was supported by ANID-FONDECYT grant #1221128 for M.I. Yuseff, ANID Ph.D. national scholarship #21191062 for F. Del Valle Batalla, and the Research Council of

Finland (grant #339810 to P.K. Mattila). F. Del Valle Batalla and M.I. Yuseff thank all members of the P.K. Mattila lab for their constructive feedback on this work. We also thank Martina Alamo from the M.I. Yuseff lab for her useful advice concerning experimental procedures and ideas for new approaches.

Author contributions: P. Aceitón: conceptualization, data curation, formal analysis, investigation, methodology, software, supervision, validation, visualization, and writing—original draft, review, and editing. I. Riobó: conceptualization, formal analysis, investigation, methodology, software, visualization, and writing—review and editing. F. Del Valle Batalla: conceptualization, formal analysis, investigation, methodology, software, and writing—original draft. J. Diaz-Muñoz: investigation, methodology, resources, and supervision. R. Ulloa: investigation and methodology. F. Cabrera Reyes: investigation and methodology. T. Contreras: investigation. S. Hernández-Pérez: investigation and writing—review and editing. P.K. Mattila: conceptualization, funding acquisition, methodology, project administration, resources, supervision, and writing—review and editing. M.I. Yuseff: conceptualization, formal analysis, funding acquisition, investigation, methodology, project administration, resources, supervision, validation, visualization, and writing—original draft, review, and editing.

Disclosures: The authors declare no competing interests exist.

Submitted: 27 July 2024
Revised: 24 March 2025
Accepted: 23 May 2025

References

Akkaya, M., K. Kwak, and S.K. Pierce. 2020. B cell memory: Building two walls of protection against pathogens. *Nat. Rev. Immunol.* 20:229–238. https://doi.org/10.1038/s41577-019-0244-2

Bance, B., S. Seetharaman, C. Leduc, B. Boëda, and S. Etienne-Manneville. 2019. Microtubule acetylation but not detyrosination promotes focal adhesion dynamics and astrocyte migration. *J. Cell Sci.* 132:jcs225805. https://doi.org/10.1242/jcs.225805

Barral, D.C., L. Staiano, C. Guimas Almeida, D.F. Cutler, E.R. Eden, C.E. Futter, A. Galione, A.R.A. Marques, D.L. Medina, G. Napolitano, et al. 2022. Current methods to analyze lysosome morphology, positioning, motility and function. *Traffic*. 23:238–269. https://doi.org/10.1111/tra.12839

Basu, R., B.M. Whitlock, J. Husson, A. Le Floc'h, W. Jin, A. Oyler-Yaniv, F. Dotiwala, G. Giannone, C. Hivroz, N. Biais, et al. 2016. Cytotoxic T cells use mechanical force to potentiate target cell killing. *Cell*. 165:100–110. https://doi.org/10.1016/j.cell.2016.01.021

Basu, R., and M. Huse. 2017. Mechanical communication at the immunological synapse. *Trends Cell Biol.* 27:241–254. https://doi.org/10.1016/j.tcb.2016.10.005

Bhuwania, R., A. Castro-Castro, and S. Linder. 2014. Microtubule acetylation regulates dynamics of KIF1C-powered vesicles and contact of microtubule plus ends with podosomes. *Eur. J. Cell Biol.* 93:424–437. https://doi.org/10.1016/j.ejcb.2014.07.006

Bouzid, T., E. Kim, B.D. Riehl, A.M. Esfahani, J. Rosenbohm, R. Yang, B. Duan, and J.Y. Lim. 2019. The LINC complex, mechanotransduction, and mesenchymal stem cell function and fate. *J. Biol. Eng.* 13:68. https://doi.org/10.1186/s13036-019-0197-9

Bufi, N., M. Saitakis, S. Dogniaux, O. Buschinger, A. Bohineust, A. Richert, M. Maurin, C. Hivroz, and A. Asnacios. 2015. Human primary immune cells exhibit distinct mechanical properties that are modified by inflammation. *Biophys. J.* 108:2181–2190. https://doi.org/10.1016/j.bpj.2015.03.047

Cabrera-Reyes, F., T. Contreras-Palacios, R. Ulloa, J. Jara-Wilde, M. Caballero, C. Quiroga, C.G. Feijoo, J. Díaz-Muñoz, and M.-I. Yuseff. 2024. SNX5 promotes antigen presentation in B cells by dual regulation of actin and lysosomal dynamics. *Life Sci. Alliance*. 8. e202402917. https://doi.org/10.26508/lsa.202402917

Carrasco, Y.R., and F.D. Batista. 2007. B cells acquire particulate antigen in a macrophage-rich area at the boundary between the follicle and the subcapsular sinus of the lymph node. *Immunity*. 27:160–171. https://doi.org/10.1016/j.immuni.2007.06.007

Charrier, E.E., K. Pogoda, R. Li, C.Y. Park, J.J. Fredberg, and P.A. Janmey. 2020. A novel method to make viscoelastic polyacrylamide gels for cell culture and traction force microscopy', *APL Bioeng.* 4:036104. https://doi.org/10.1063/5.0002750

Cheng, B., M. Li, W. Wan, H. Guo, G.M. Genin, M. Lin, and F. Xu. 2023. Predicting YAP/TAZ nuclear translocation in response to ECM mechanosensing. *Biophys. J.* 122:49–63. https://doi.org/10.1016/j.bpj.2022.11.2943

Chen, Y., L. Ju, M. Rushdi, C. Ge, and C. Zhu. 2017. Receptor-mediated cell mechanosensing. *Mol. Biol. Cell*. 28:3134–3155. https://doi.org/10.1091/mbc.E17-04-0228

Ciechomska, M., C.L. Wilson, A. Floudas, W. Hui, A.D. Rowan, W. van Eden, J.H. Robinson, and A.M. Knight. 2014. Antigen-specific B lymphocytes acquire proteoglycan aggrecan from cartilage extracellular matrix resulting in antigen presentation and $CD4^+$ T-cell activation. *Immunology*. 141:70–78. https://doi.org/10.1111/imm.12169

Corrales Vázquez, O., T. Contreras, M. Alamo Rollandi, F. Del Valle Batalla, and M.-I. Yuseff. 2025. Quantitative analysis of the B cell immune synapse using imaging techniques. *Methods Cell Biol.* 193:229–252. https://doi.org/10.1016/bs.mcb.2023.08.002

Deb Roy, A., E.G. Gross, G.S. Pillai, S. Seetharaman, S. Etienne-Manneville, and T. Inoue. 2022. Non-catalytic allostery in α-TAT1 by a phosphoswitch drives dynamic microtubule acetylation. *J. Cell Biol.* 221:e202202100. https://doi.org/10.1083/jcb.202202100

Dunn, S., E.E. Morisson, T.B. Liverpool, C. Molina-París, R.A. Cross, M.C. Alonso, and M. Peckham. 2008. Differential trafficking of Kif5c on tyrosinated and detyrosinated microtubules in live cells. *J. Cell Sci.* 121:1085–1095. https://doi.org/10.1242/jcs.026492

Even, A., G. Morelli, L. Broix, C. Scaramuzzino, S. Turchetto, I. Gladwyn-Ng, R. Le Bail, M. Shilian, S. Freeman, M.M. Magiera, et al. 2019. ATAT1-enriched vesicles promote microtubule acetylation via axonal transport. *Sci. Adv.* 5:eaax2705. https://doi.org/10.1126/sciadv.aax2705

Fine, N., I.D. Dimitriou, J. Rullo, M.J. Sandí, B. Petri, J. Haitsma, H. Ibrahim, J. La Rose, M. Glogauer, P. Kubes, et al. 2016. GEF-H1 is necessary for neutrophil shear stress–induced migration during inflammation. *J. Cell Biol.* 215:107–119. https://doi.org/10.1083/jcb.201603109

Fleire, S.J., J.P. Goldman, Y.R. Carrasco, M. Weber, D. Bray, and F.D. Batista. 2006. B cell ligand discrimination through a spreading and contraction response. *Science*. 312:738–741. https://doi.org/10.1126/science.1123940

Friedman, D., P. Simmonds, A. Hale, L. Bere, N.W. Hodson, M.R.H. White, and D.M. Davis. 2021. Natural killer cell immune synapse formation and cytotoxicity are controlled by tension of the target interface. *J. Cell Sci.* 134:jcs258570. https://doi.org/10.1242/jcs.258570

Grune, T., R. Kehm, A. Höhn, T. Jung. 2018. "Cyt/Nuc," a customizable and documenting ImageJ macro for evaluation of protein distributions between cytosol and nucleus. *Biotechnol. J.* 13:e1700652. https://doi.org/10.1002/biot.201700652

Hoogeboom, R., and P. Tolar. 2016. Molecular mechanisms of B cell antigen gathering and endocytosis. *In B Cell Receptor Signaling*. T. Kurosaki, and J. Wienands, editors. Springer International Publishing, Cham. 45–63. https://doi.org/10.1007/82_2015_476

Ibañez-Vega, J., F. Del Valle Batalla, J.J. Saez, A. Soza, and M. Yuseff. 2019a. Proteasome dependent actin remodeling facilitates antigen extraction at the immune synapse of B cells. *Front. Immunol.* 10:225. https://doi.org/10.3389/fimmu.2019.00225

Ibañez-Vega, J., D. Fuentes, J. Lagos, J. Cancino, and M.I. Yuseff. 2019b. Studying organelle dynamics in B cells during immune synapse formation. *J. Vis. Exp.* https://doi.org/10.3791/59621

Janke, C., and M.M. Magiera. 2020. The tubulin code and its role in controlling microtubule properties and functions. *Nat. Rev. Mol. Cell Biol.* 21:307–326. https://doi.org/10.1038/s41580-020-0214-3

Kim, T.-H., C. Ly, A. Christodoulides, C.J. Nowell, P.W. Gunning, E.K. Sloan, and A.C. Rowat. 2019. Stress hormone signaling through β-adrenergic receptors regulates macrophage mechanotype and function. *FASEB J.* 33:3997–4006. https://doi.org/10.1096/fj.201801429rr

Kudo, N., B. Wolff, T. Sekimoto, E.P. Schreiner, Y. Yoneda, M. Yanagida, S. Horinouchi, and M. Yoshida. 1998. Leptomycin B inhibition of signal-mediated nuclear export by direct binding to CRM1. *Exp. Cell Res.* 242: 540–547. https://doi.org/10.1006/excr.1998.4136

Lachowski, D., C. Matellan, S. Gopal, E. Cortes, B.K. Robinson, A. Saiani, A.F. Miller, M.M. Stevens, and A.E. Del Río Hernández. 2022. Substrate stiffness-driven membrane tension modulates vesicular trafficking via Caveolin-1. *ACS Nano*. 16:4322–4337. https://doi.org/10.1021/acsnano.1c10534

Li, X., J.D. Combs, 3rd, K. Salaita, and X. Shu. 2023. Polarized focal adhesion kinase activity within a focal adhesion during cell migration. *Nat. Chem. Biol.* 19:1458–1468. https://doi.org/10.1038/s41589-023-01353-y

Liu, C., M.K. Fallen, H. Miller, A. Upadhyaya, and W. Song. 2013. The actin cytoskeleton coordinates the signal transduction and antigen processing functions of the B cell antigen receptor. *Front. Biol.* 8:475–485. https://doi.org/10.1007/s11515-013-1272-0

Maiuri, P., J.-F. Rupprecht, S. Wieser, V. Ruprecht, O. Bénichou, N. Carpi, M. Coppey, S. De Beco, N. Gov, C.-P. Heisenberg, et al. 2015. Actin flows mediate a universal coupling between cell speed and cell persistence. *Cell*. 161:374–386. https://doi.org/10.1016/j.cell.2015.01.056

Mandal, S., M. Melo, P. Gordiichuk, S. Acharya, Y.-C. Poh, N. Li, A. Aung, E.L. Dane, D.J. Irvine, and S. Kumari. 2023. WASP facilitates tumor mechanosensitivity in T lymphocytes. WASP facilitates tumor mechanosensitivity in T lymphocytes. *Elife*. 12:RP91854. https://doi.org/10.7554/eLife.91854.1

Montagnac, G., V. Meas-Yedid, M. Irondelle, A. Castro-Castro, M. Franco, T. Shida, M.V. Nachury, A. Benmerah, J.-C. Olivo-Marin, and P. Chavrier. 2013. αTAT1 catalyses microtubule acetylation at clathrin-coated pits. *Nature*. 502:567–570. https://doi.org/10.1038/nature12571

Morelli, G., A. Even, I. Gladwyn-Ng, R. Le Bail, M. Shilian, J.D. Godin, E. Peyre, B.A. Hassan, A. Besson, J.-M. Rigo, et al. 2018. p27Kip1 modulates axonal transport by regulating α-Tubulin acetyltransferase 1 stability. *Cell Rep.* 23:2429–2442. https://doi.org/10.1016/j.celrep.2018.04.083

Núñez-Andrade, N., S. Iborra, A. Trullo, O. Moreno-Gonzalo, E. Calvo, E. Catalán, G. Menasche, D. Sancho, J. Vázquez, T.P. Yao, et al. 2016. HDAC6 regulates the dynamics of lytic granules in cytotoxic T lymphocytes. *J. Cell Sci.* 129:1305–1311. https://doi.org/10.1242/jcs.180885

Obino, D., J. Diaz, J.J. Sáez, J. Ibañez-Vega, P.J. Sáez, M. Alamo, D. Lankar, and M.-I. Yuseff. 2017. Vamp-7–dependent secretion at the immune synapse regulates antigen extraction and presentation in B-lymphocytes. *Mol. Biol. Cell*. 28:890–897. https://doi.org/10.1091/mbc.E16-10-0722

Panciera, T., L. Azzolin, M. Cordenonsi, and S. Piccolo. 2017. Mechanobiology of YAP and TAZ in physiology and disease. *Nat. Rev. Mol. Cell Biol.* 18: 758–770. https://doi.org/10.1038/nrm.2017.87

Pathni, A., K. Wagh, I. Rey-Suarez, and A. Upadhyaya. 2024. Mechanical regulation of lymphocyte activation and function. *J. Cell Sci.* 137: jcs219030. https://doi.org/10.1242/jcs.219030

Phuyal, S., E. Djaerff, A.-L. Le Roux, M.J. Baker, D. Fankhauser, S.J. Mahdizadeh, V. Reiterer, A. Parizadeh, E. Felder, J.C. Kahlhofer, et al. 2022. Mechanical strain stimulates COPII-Dependent secretory trafficking via Rac1. *EMBO J.* 41:e110596. https://doi.org/10.15252/embj.2022110596

Pineau, J., L. Pinon, O. Mesdjian, J. Fattaccioli, A.-M. Lennon-Duménil, and P. Pierobon. 2022. Microtubules restrict F-actin polymerization to the immune synapse via GEF-H1 to maintain polarity in lymphocytes. *Elife*. 11:e78330. https://doi.org/10.7554/eLife.78330

Pu, J., C.M. Guardia, T. Keren-Kaplan, and J.S. Bonifacino. 2016. Mechanisms and functions of lysosome positioning. *J. Cell Sci.* 129:4329–4339. https://doi.org/10.1242/jcs.196287

Riobó, I., and M.I. Yuseff. 2024. B cell mechanosensing regulates ER remodeling at the immune synapse. *Front. Immunol.* 15:1464000. https://doi.org/10.3389/fimmu.2024.1464000

Rogers, J., A.T. Bajur, K. Salaita, and K.M. Spillane. 2024. Mechanical control of antigen detection and discrimination by T and B cell receptors. *Biophys. J.* 123:2234–2255. https://doi.org/10.1016/j.bpj.2024.05.020

Rocha, N., and J. Neefjes. 2008. MHC class II molecules on the move for successful antigen presentation. *EMBO J.* 27:1–5. https://doi.org/10.1038/sj.emboj.7601945

Roper, S.I., L. Wasim, D. Malinova, M. Way, S. Cox, and P. Tolar. 2019. B cells extract antigens at Arp2/3-generated actin foci interspersed with linear filaments. *Elife*. 8:e48093. https://doi.org/10.7554/eLife.48093

Sáez, J.J., J. Diaz, J. Ibañez, J.P. Bozo, F. Cabrera Reyes, M. Alamo, F.-X. Gobert, D. Obino, M.R. Bono, A.-M. Lennon-Duménil, et al. 2019. The exocyst controls lysosome secretion and antigen extraction at the immune synapse of B cells. *J. Cell Biol.* 218:2247–2264. https://doi.org/10.1083/jcb.201811131

Schindelin, J., I. Arganda-Carreras, E. Frise, V. Kaynig, M. Longair, T. Pietzsch, S. Preibisch, C. Rueden, S. Saalfeld, B. Schmid, et al. 2012. Fiji: An open-source platform for biological-image analysis. *Nat. Methods*. 9: 676–682. https://doi.org/10.1038/nmeth.2019

Seetharaman, S., B. Vianay, V. Roca, A.J. Farrugia, C. De Pascalis, B. Boëda, F. Dingli, D. Loew, S. Vassilopoulos, A. Bershadsky, et al. 2022. Microtubules tune mechanosensitive cell responses. *Nat. Mater.* 21:366–377. https://doi.org/10.1038/s41563-021-01108-x

Serra-Marques, A., M. Martin, E.A. Katrukha, I. Grigoriev, C.A. Peeters, Q. Liu, P.J. Hooikaas, Y. Yao, V. Solianova, I. Smal, et al. 2020. Concerted action of kinesins kif5b and kif13b promotes efficient secretory vesicle transport to microtubule plus ends. *Elife*. 9:e61302. https://doi.org/10.7554/eLife.61302

Shaheen, S., Z. Wan, Z. Li, A. Chau, X. Li, S. Zhang, Y. Liu, J. Yi, Y. Zeng, J. Wang, et al. 2017. Substrate stiffness governs the initiation of B cell activation by the concerted signaling of PKCβ and focal adhesion kinase. *Elife*. 6:e23060. https://doi.org/10.7554/eLife.23060

Shaheen, S., Z. Wan, K. Haneef, Y. Zeng, W. Jing, and W. Liu. 2019. B cell mechanosensing: A mechanistic overview. Adv. Immunol. 144:23–63. https://doi.org/10.1016/bs.ai.2019.08.003

Tang, M., B. Chen, H. Xia, M. Pan, R. Zhao, J. Zhou, Q. Yin, F. Wan, Y. Yan, C. Fu, et al. 2023. pH-gated nanoparticles selectively regulate lysosomal function of tumour-associated macrophages for cancer immunotherapy. *Nat. Commun.* 14:5888. https://doi.org/10.1038/s41467-023-41592-0

Trappmann, B., J.E. Gautrot, J.T. Connelly, D.G.T. Strange, Y. Li, M.L. Oyen, M.A. Cohen Stuart, H. Boehm, B. Li, V. Vogel, et al. 2012. Extracellular-matrix tethering regulates stem-cell fate. *Nat. Mater.* 11:642–649. https://doi.org/10.1038/nmat3339

Takata, T., and M. Matsumura. 2022. The LINC complex assists the nuclear import of mechanosensitive transcriptional regulators. *In Nuclear, Chromosomal, and Genomic Architecture in Biology and Medicine. Results and Problems in Cell Differentiation*. Vol. 70. M. Kloc, and J.Z. Kubiak, editors. Springer International Publishing, Cham. 315–337. https://doi.org/10.1007/978-3-031-06573-6_11

Ulloa, R., O. Corrales, F. Cabrera-Reyes, J. Jara-Wilde, J.J. Saez, C. Rivas, J. Lagos, S. Härtel, C. Quiroga, M.-I. Yuseff, and J. Diaz-Muñoz. 2021. B cells adapt their nuclear morphology to organize the immune synapse and facilitate antigen extraction. *Front. Immunol.* 12:801164. https://doi.org/10.3389/fimmu.2021.801164

Wan, Z., S. Zhang, Y. Fan, K. Liu, F. Du, A.M. Davey, H. Zhang, W. Han, C. Xiong, and W. Liu. 2013. B cell activation is regulated by the stiffness properties of the substrate presenting the antigens. *J. Immunol.* 190: 4661–4675. https://doi.org/10.4049/jimmunol.1202976

Wang, M.S., Y. Hu, E.E. Sanchez, X. Xie, N.H. Roy, M. de Jesus, B.Y. Winer, E.A. Zale, W. Jin, C. Sachar, et al. 2022. Mechanically active integrins target lytic secretion at the immune synapse to facilitate cellular cytotoxicity. *Nat. Commun.* 13:3222. https://doi.org/10.1038/s41467-022-30809-3

Wang, G., S.S. Nola, S. Bovio, M. Coppey-Moisan, F. Lafont, and T. Galli. 2018. Biomechanical control of lysosomal secretion via the VAMP7 hub: A tug-of-war mechanism between VARP and LRRK1. *iScience*. 4:127–143, https://doi.org/10.1016/j.isci.2018.05.016

Wang, J.C., Y.-I. Yim, X. Wu, V. Jaumouille, A. Cameron, C.M. Waterman, J.H. Kehrl, and J.A. Hammer. 2022. A B-cell actomyosin arc network couples integrin co-stimulation to mechanical force-dependent immune synapse formation. *Elife*. 11:e72805. https://doi.org/10.7554/eLife.72805

Yuseff, M.-I., A. Reversat, D. Lankar, J. Diaz, I. Fanget, P. Pierobon, V. Randrian, N. Larochette, F. Vascotto, C. Desdouets, et al. 2011. Polarized secretion of lysosomes at the B cell synapse couples antigen extraction to processing and presentation. *Immunity*. 35:361–374. https://doi.org/10.1016/j.immuni.2011.07.008

Yuseff, M.-I., P. Pierobon, A. Reversat, and A.-M. Lennon-Duménil. 2013. How B cells capture, process and present antigens: A crucial role for cell polarity. *Nat. Rev. Immunol.* 13:475–486. https://doi.org/10.1038/nri3469

Zhu, C., W. Chen, J. Lou, W. Rittase, and K. Li. 2019a. Mechanosensing through immunoreceptors. *Nat. Immunol.* 20:1269–1278. https://doi.org/10.1038/s41590-019-0491-1

Zhu, C., Y. Chen, and L.A. Ju. 2019b. Dynamic bonds and their roles in mechanosensing. *Curr. Opin. Chem. Biol.* 53:88–97. https://doi.org/10.1016/j.cbpa.2019.08.005

Supplemental material

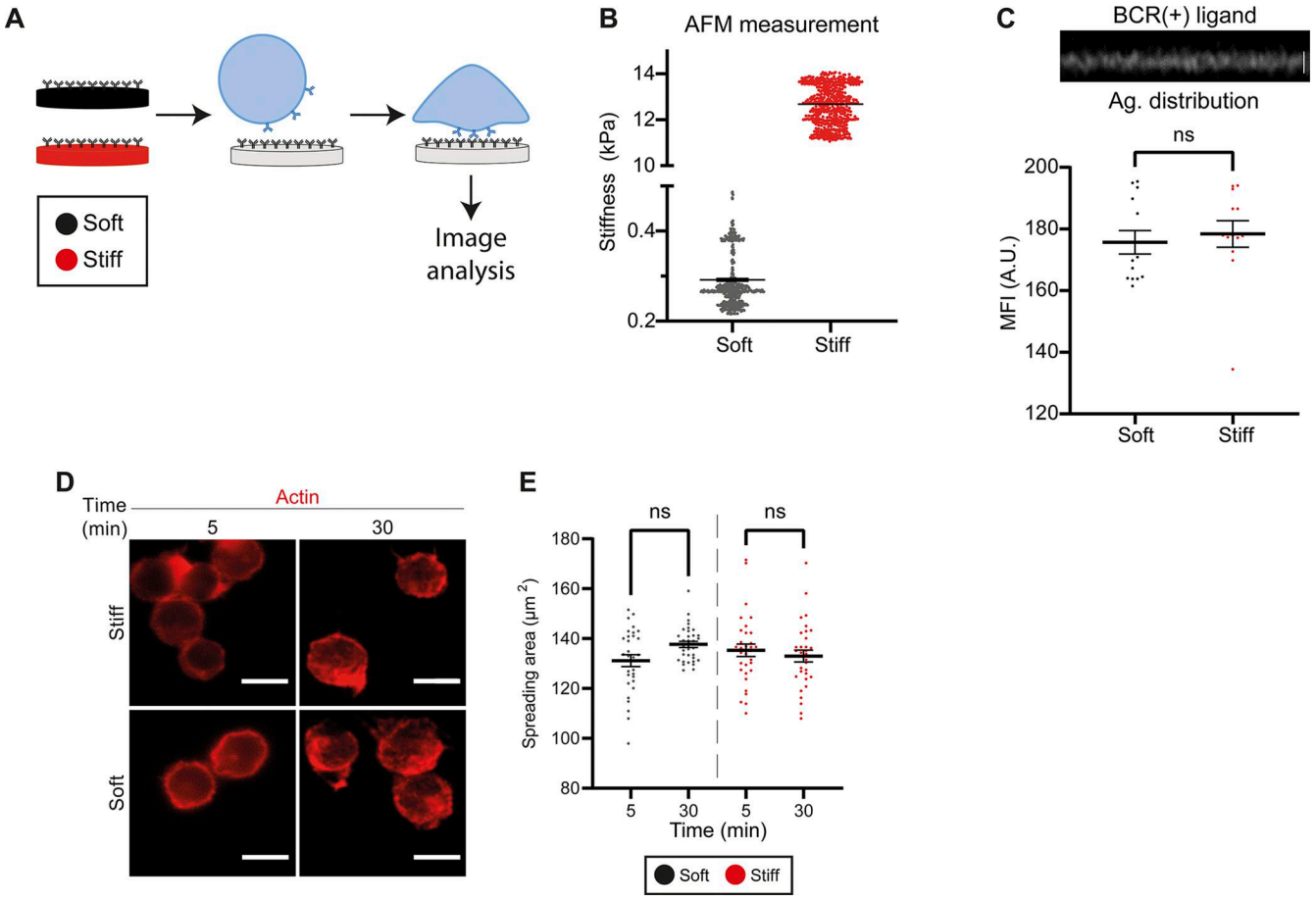

Figure S1. **B cell spreading in response to substrate stiffness depends on BCR activation and is unaffected by stiffness alone. (A)** Illustration of basic workflow used to activate B cells on PAA gels. Cells are seeded for different time points and then fixed, used for live imaging, or lysed for protein extraction. **(B)** AFM measurements in kPA of gel stiffness. Soft gels have values of 0.3 kPa, and stiff, 13 kPa. **(C)** Top: Representative confocal image for the Z cross section of a PAA gel coupled to a fluorescently labeled BCR^+ ligand. Scale bar: 2 µm. Bottom: Analysis for antigen distribution (BCR^+ ligand) based on MFI values acquired in confocal microscopy. **(D)** Representative images of B cells seeded on soft and stiff gels coupled to a BCR^- ligand (nonactivating). Cells were labeled with phalloidin (red) and do not display spreading responses. Scale bar: 5 µm. **(E)** Quantification of the spreading area from experiments depicted in D. Shown data consider $n \geq 30$ cells pooled from $N = 3$, independent experiments. **(E)**: Two-way ANOVA with Sidak's multiple comparison test. **(B and C)**: *t* test. P values illustrated with asterisks are * <0.05 and *** <0.001.

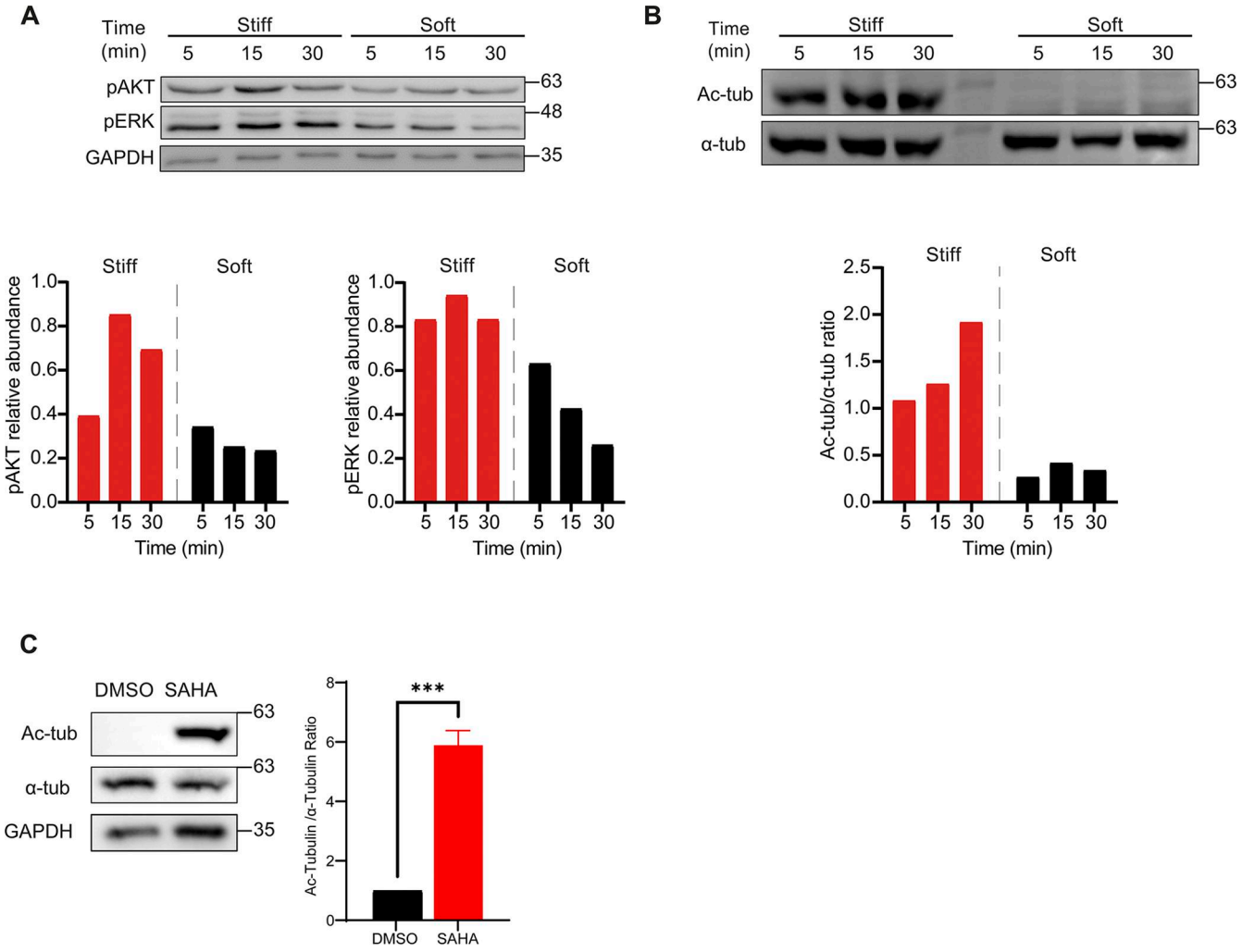

Figure S2. **B cells activated on stiff substrates display enhanced BCR signaling and microtubule acetylation. (A and B)** Top: Western blot of B cells activated on soft and stiff surfaces for different time points to measure pAKT, pERK, and GAPDH (A), or Ac-Tub (B). Bottom: Quantifications of the relative abundance of pAKT and pERK with respect to GAPDH (A) or Ac-Tub with respect to total tubulin (B). **(C)** Western blot analysis of Ac-Tub levels in B cells treated with SAHA. Representative immunoblots showing the expression of Ac-Tub, total α-Tub, and GAPDH as a loading control in vehicle (DMSO) and SAHA-treated B cells. The quantification (right) represents the ratio of Ac-Tub to total α-Tub, normalized to the DMSO condition. *t* test. P values illustrated with asterisks are * <0.05. Source data are available for this figure: SourceData FS2.

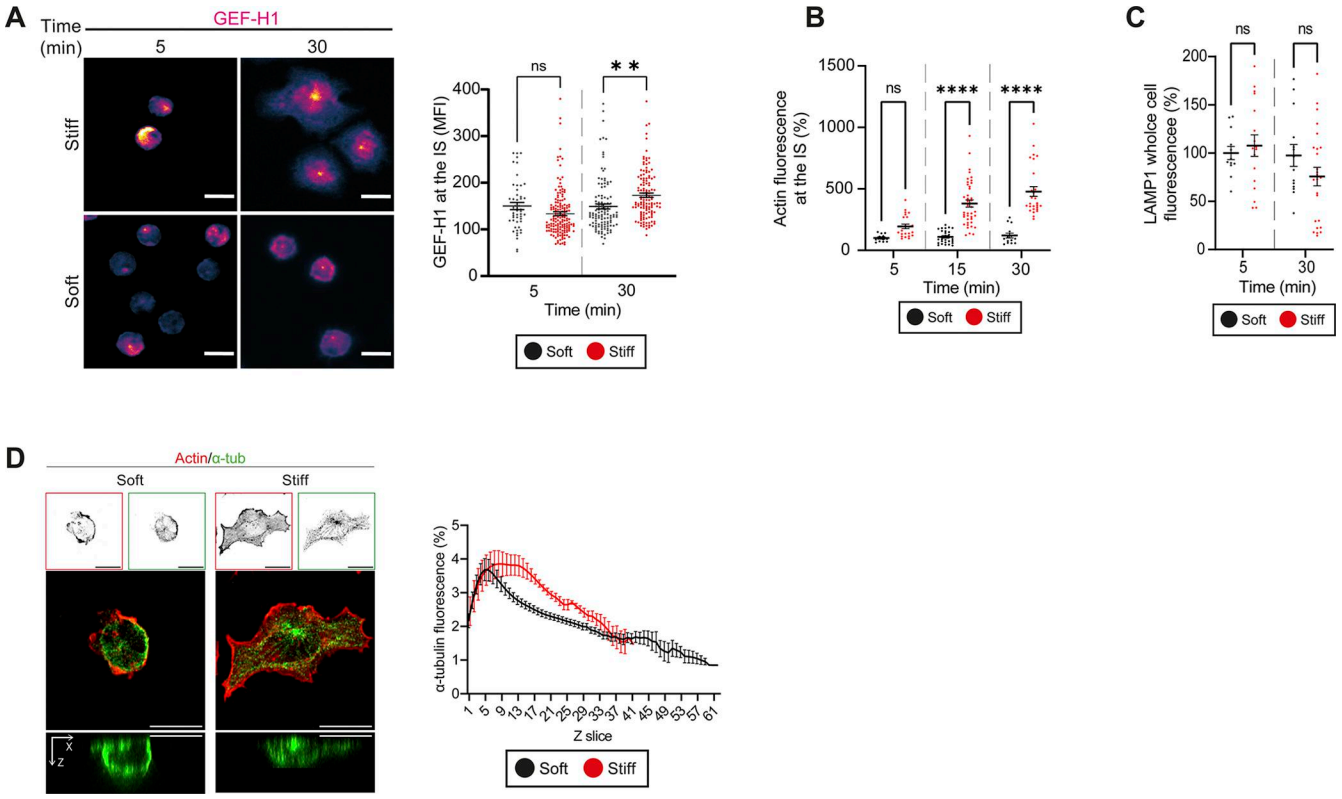

Figure S3. **Activation of B cells on stiff substrates enhances GEF-H1 recruitment and actin accumulation at the immune synapse, while MTOC polarization remains unaltered. (A)** Representative images of fixed cells activated on soft or stiff substrates at different time points and stained for GEF-H1. A fluorescence intensity of GEF-H1 is shown in a gradient of magenta. Right panel shows quantification of GEFH1 intensity at the IS for the experiments represented in A. **(B)** Quantification of actin fluorescence at the IS in B cells activated on soft or stiff substrates for 5, 15, or 30 min. **(C)** Quantification of LAMP1 fluorescence intensity in whole cells interacting with substrates of different stiffness for 5 and 30 min. **(D)** Representative confocal images of B cells on soft and stiff substrates, stained for actin (red) and α-Tub (green), including orthogonal x-z projections. Right panel shows a z-scan of α-Tub fluorescence intensity. Scale bars, 10 µm. Two-way ANOVA with Sidak's multiple comparison test. P values illustrated with asterisks are * <0.05, * <0.01, and ** <0.001.

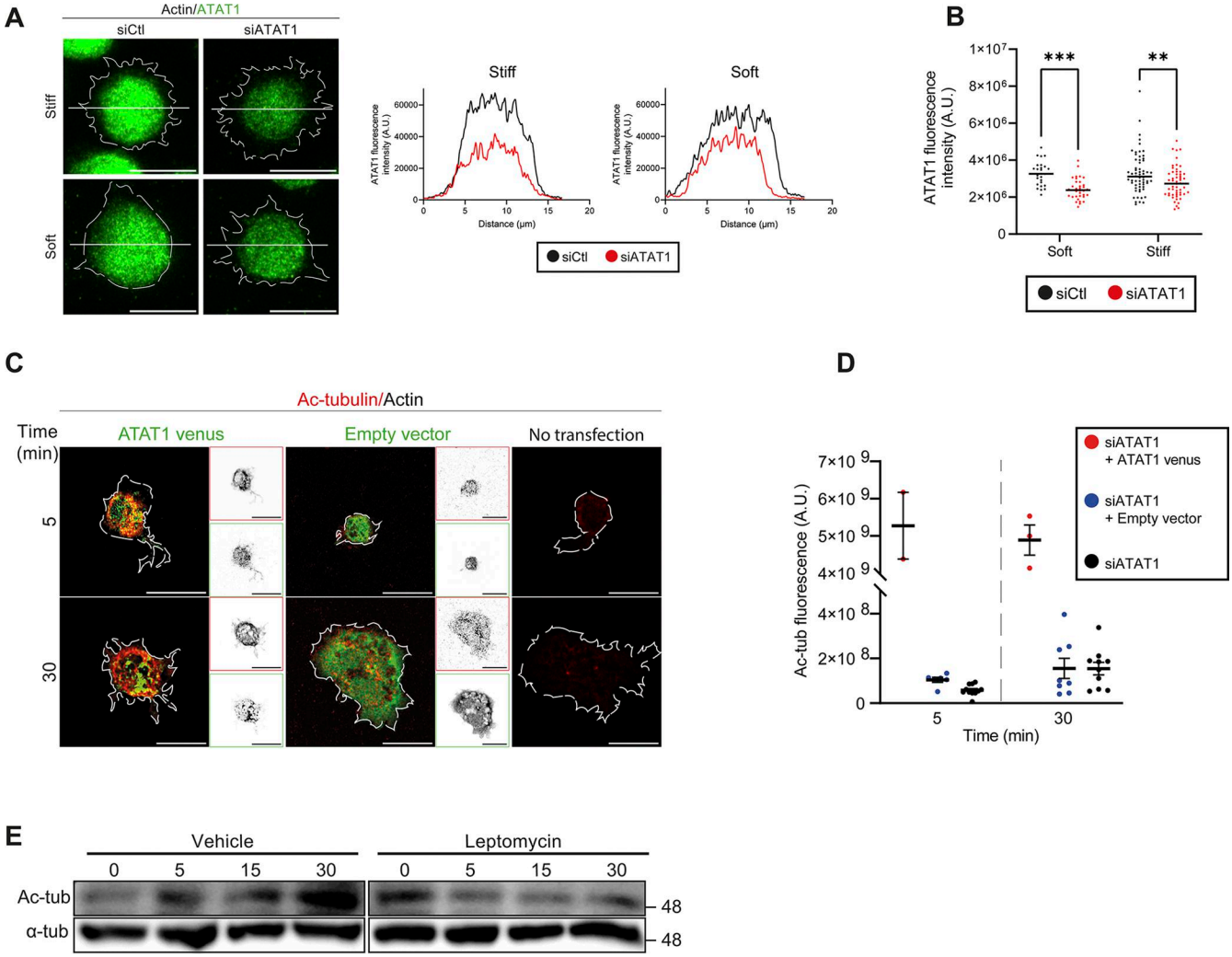

Figure S4. **Efficient silencing of ATAT1 in B cells, followed by rescue of its expression, restores tubulin acetylation, whereas leptomycin-treated B cells display reduced tubulin acetylation. (A)** Left: Representative confocal images of control (siCtl) or ATAT1-silenced (siATAT1) B cells transfected, activated on stiff or soft substrates, and stained for ATAT1 (green). White outlines indicate cell contours, obtained by F-actin staining. Right: Line-scan profiles of ATAT1 fluorescence intensity across the cell diameter. **(B)** Quantification of ATAT1 fluorescence intensity from cells shown in A. **(C)** Representative confocal images of siATAT1 B cells expressing ATAT1-venus, empty vector, or non-transfected cells, activated on glass slides coated with BCR$^+$ ligands for 5 and 10 min. **(D)** Quantification of Ac-Tub fluorescence intensity from cells shown in C. **(E)** Western blot of Ac-Tub and α-Tub (loading control) in B cells activated for 0, 5, 15, or 30 min in the presence of vehicle (EtOH) or LMB. Shown data consider $n \geq 30$ cells pooled from $N = 3$ independent experiments. Scale bars are 10 µm. Two-way ANOVA with Sidak's multiple comparison test. P values illustrated with asterisks are ** <0.01 and *** <0.001. Source data are available for this figure: SourceData FS4.

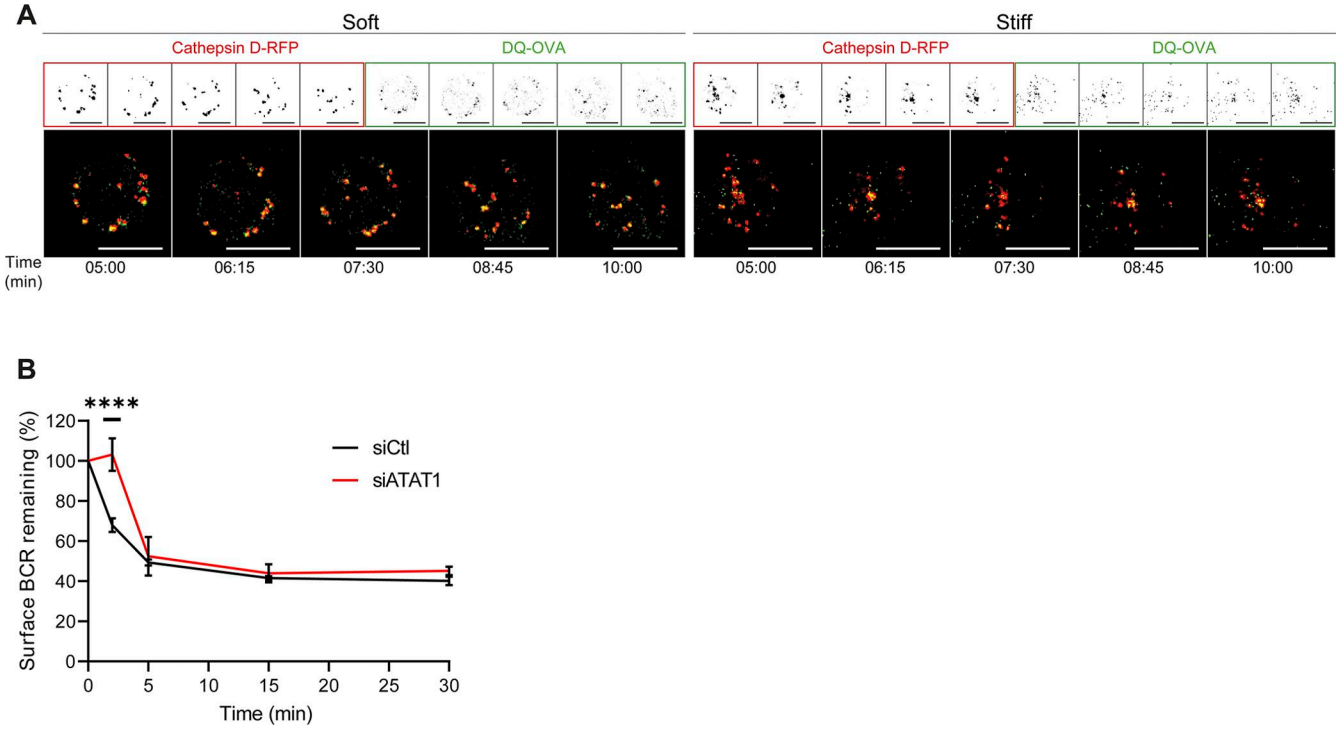

Figure S5. **B cells activated on stiff substrates show increased central lysosome clustering and activity, whereas ATAT1-silenced cells exhibit impaired BCR internalization at early time points. (A)** Representative time-lapse images of (siCtl) or (siATAT1) B cells expressing cathepsin D-RFP, activated on soft or stiff substrates coated with BCR$^+$ ligands plus DQ-OVA (green) to monitor antigen extraction. Scale bar: 10 µm. **(B)** Quantification of surface BCR levels over time in siCtl and siATAT1 B cells by flow cytometry, measured as the percentage of remaining surface BCR upon activation. Two-way ANOVA with Sidak's multiple comparison test. P values illustrated with asterisks are **** <0.0001.

Video 1. **Lysosomal dynamics in B cells activated on soft or stiff substrates.** Time-lapse video of B cells expressing cathepsin D-RFP seeded on soft and stiff substrates containing BCR$^+$ ligands. Imaging was performed 15 min after seeding and acquired every 8 s over a 5-min period.

Video 2. **Lysosome dynamics in B cells activated on soft or stiff substrates in the presence or absence of the histone deacetylase inhibitor (SAHA).** Time-lapse video showing B cells expressing cathepsin-D-RFP (grayscale) seeded on soft or stiff substrates containing BCR$^+$ ligands. Cells were either left untreated (NT) or pretreated with 1 µM SAHA for 30 min. Imaging was initiated 15 min after seeding and acquired every 8 s over a 5-min period.